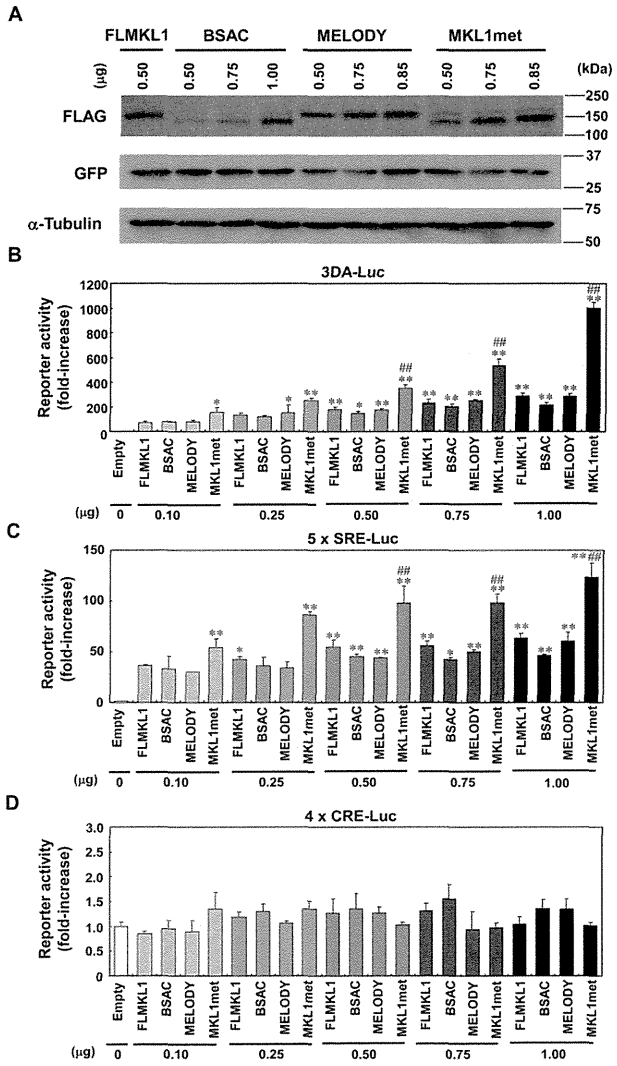

Fig. 4. Effects of MKL1 isoforms on SRF- and CREB-mediated transcriptional responses in NIH3T3 cells. (A) The expression level of FLAG-tagged MKL1 variants. FLAG-tagged FLMKL1, BSAC, MELODY or MKL1met (the amount indicated as 0.50–1.00) was co-transfected with GFP vector (1 μg/well) into NIH3T3 cells. Twenty-four hours later, cell lysates were collected and Western blotting was performed. In transfection studies presented in this and subsequent figures, empty vector was added as needed to keep the total amount of expression vectors used for transfection per well constant. (B–D) Either 1.0 μg/well of empty vector (Empty), 0.1, 0.25, 0.5, 0.75 and 1.0 μg/well of FLAG-tagged FLMKL1, BSAC, MELODY or MKL1met was co-transfected with firefly luciferase vector (B: 3D.A.Luc, C: 5 × SRE-Luc, D: 4 × CRE-Luc, 1.0 μg/well) and Renilla luciferase reporter vectors, TK-Renilla (0.2 μg/well) into NIH3T3 cells. Twenty-four hours later, luciferase activities were measured. To keep the total amount of transfected vector constant (2 μg total/well), empty vector was added as needed. Bar graphs represent the means ± SD from at least three samples. $^{*}p < 0.05$ (vs. empty), $^{**}p < 0.01$ (vs. empty), $^{***}p < 0.001$ (vs. empty), $^{\#\#}p < 0.01$ (vs. FLMKL1).

were derived from cDNA, but not from contamination with genomic DNA. Furthermore, only one band was generated in each assay and it had the predicted size, suggesting that the quantitative PCR analysis specifically detected only one amplified band of interest, but not non-specific bands. Two initiator codons of FLMKL1 give rise to two translation products, FLMKL1 and MKL1met. Therefore, the PCR products amplified with primers for FLMKL1 included both FLMKL1 and MKL1met. Quantitative real-time PCR revealed that all MKL1 transcripts were enriched in the nervous system (Fig. 2) and that the level of MELODY mRNA was very low compared to other transcripts (Fig. 2C). As expression of MELODY is orders of magnitude below that of FLMKL1 and BSAC, its impact on cell signaling is unclear. The expression of FLMKL1 and MELODY was relatively high in the testis and the olfactory bulb (Fig. 2A and C). BSAC was enriched in the hippocampus (Fig. 2B).

3.3. Developmental regulation of rat MKL1 transcripts in the brain

As the tissue survey described above showed that MKL1 mRNA was highly expressed in the brain (Fig. 2), we proceeded to determine the expression profile of MKL1 transcripts during brain development. Using quantitative PCR analysis of cDNAs derived from several brain regions at different developmental stages, we found that BSAC was the most abundant of the three MKL1 transcripts during brain development (Fig. 3). The expression level of BSAC mRNA increased after P10–P15 in both the hippocampus and the cerebral cortex (Fig. 3H and K). In contrast, MELODY mRNA level decreased during development in several brain regions (Fig. 3C, I, L and O). The expression pattern of FLMKL1 mRNA during development varied across different regions (Fig. 3A, D, G, J and M). In combination, these data show that the pattern of expression of the alternative transcripts generated from the rat MKL1 gene is dynamically regulated during brain development.

3.4. SRF coactivator function of rat MKL1 isoforms

Next, we examined the functional activities of MKL1 isoforms in NIH3T3 cells. We first checked the expression level of FLAG-tagged MKL1 isoforms. As shown in Fig. 4A, the expression levels of MKL1 isoforms were varied when 0.50–1.00 μg of FLAG-MKL1 expression vectors were transfected. Likewise, we also checked the effects of these four MKL1 isoforms on SRF-mediated transcriptional responses in NIH3T3 cells. All four MKL1 isoforms increased SRF-mediated transcriptional responses (Fig. 4B and C). When the same amounts of MKL1 expression vector were transfected into NIH3T3 cells, MKL1met was the most effective in driving SRF-mediated transcription among the four MKL1 isoforms. On the other hand, all four MKL1 isoforms did not activate cAMP response element (CRE)-mediated transcription significantly in NIH3T3 cells (Fig. 4D).

4. Discussion

In this study, we have identified three transcripts generated from the rat MKL1 gene: two of these, FLMKL1 and BSAC are homologous to mouse MKL1 transcripts, while the third, MELODY, represents a novel transcript (Fig. 1). Analysis of the exon–intron structure of these transcripts demonstrated that each has a distinct 5′-exon, implying that their transcription may be regulated separately by alternative promoters. Searching transcription factor-binding sites revealed that candidate binding sites of transcription factors located upstream of 5′-ends of rat MKL1 isoforms were different. This indicates that different transcription factors may be involved in the transcription of MKL1 isoforms in a spatiotemporal manner. In fact, analysis of their expression profiles revealed that all three MKL1 transcripts are enriched in the nervous system and display distinct spatiotemporal patterns of expression during brain development (Figs. 2 and 3). In terms of expression levels, there was a marked difference among the three MKL1 transcripts; in particular, the expression of MELODY is substantially lower than the other two transcripts (Figs. 2 and 3). Therefore, the influence of endogenous MELODY on SRF-mediated transcription under basal conditions may be negligible.

The functional properties of rat MKL1 isoforms indicates that the novel MKL1 isoform, MELODY, in addition to rat FLMKL1, BSAC, MKL1met isoforms strongly enhanced SRF coactivation (Fig. 4B and C). Analysis of the domain structure of the proteins generated from these MKL1 transcripts indicate that FLMKL1, BSAC and MELODY have three G-actin-binding RPEL motifs, while MKL1met has two RPEL motifs (Fig. 1). Comparison in every amount of MKL1 isoform vectors showed that MKL1met tends to be more active than other isoforms. Three RPEL motifs in a single MKL1 molecule appear to bind

to five G-actins [14]. Assuming that loss of one of these RPEL motifs decreases the stoichiometry and/or affinity of the interaction of MKL1 met with G-actin, may promote the nuclear localization, and may cause stronger activity of SRF coactivator function. In this study, we evaluated the effect of overexpressed MKL1 isoforms in NIH3T3 cells. Thus, further studies would be required for identification and function of endogenous MKL1met protein in a variety of cell types and tissues.

Although we have identified rat MKL1 isoforms, it is important to note that additional MKL1 isoforms may remain to be identified. Stern et al. [15] indicate that an MAL/MKL1 variant of relatively small size (approximately 65 kDa) is expressed in neurons. Since the rat MKL1 variants identified in this study are much larger, this smaller variant may represent another rat MKL1 variant that remains to be characterized. Further studies are needed to determine if this putative ~65 kDa form is generated from a distinct transcript or via alternative translation of one of the three transcripts described herein.

Analysis of another SRF coactivator, myocardin, [16] has demonstrated that alternative splicing gives rise to myocardin protein isoforms with different N-termini, a region that contains RPEL motifs [17]. Notably, differences in this N-terminal region affect binding of myocardin to myocyte enhancer factor 2 (MEF2), thereby regulating MEF2-mediated transcription [17]. In a similar vein, it is conceivable that the different N-termini found in MKL1 isoforms may also mediate their differential interaction with other transcription factors. To clarify the functional role of the distinct N-terminal regions of MKL1 isoforms, further studies aimed at searching for interacting proteins or at examining isoform-specific knock down by RNA interference may be valuable.

In summary, we have identified a set of rat MKL1 transcripts that are differentially expressed in developing and mature brain. Our previous study demonstrated that SRF-target β-actin gene promoter was increased by overexpression of mouse MKL1 and MKL2 in primary cultured cortical neurons [12]. To precisely investigate differential effects of MKL1 isoforms on endogenous SRF-target genes, the rescue experiments with overexpression of MKL1 isoforms in the cells, derived from MKL1 knock-out mice, might be needed. Taken together, our findings suggest that expression of multiple MKL1 isoforms helps to fine tune changes in gene expression in both developing and mature brain.

Conflict of interest

The authors have no competing financial interest or further conflict of interest.

Acknowledgements

This study was supported by a grant-in aid from the Ministry of Education, Culture, Sports, Science and Technology of Japan (Project No. 17790055, 19790052 and 22590080, A.T.; 20390023, M.T.; 23890065, M.I.) and by research grants from the Hayashi Memorial Foundation for Female Natural Scientists (A.T.), Foundation of the first Bank of Toyama (A.T.), Takeda Science Foundation (A.T.), Narishige Neuroscience Research Foundation (A.T.) and the Research Foundation for Pharmaceutical Sciences (A.T.).

Supplementary material

Supplementary material associated with this article can be found, in the online version, at doi:10.1016/j.fob.2013.09.001.

References

[1] Wang, D.Z., Li, S., Hockmeyer, D., Sutherland, L., Wang, Z., Schratt, G. et al. (2002) Potentiation of serum response factor activity by a family of myocardin-related transcription factors. Proc. Nat. Acad. Sci. USA 99, 14855–14860.
[2] Sasazuki, T., Sawada, T., Sakon, S., Kitamura, T., Kishi, T., Okazaki, T. et al. (2002) Identification of a novel transcriptional activator, BSAC, by a functional cloning to inhibit tumor necrosis factor-induced cell death. J. Biol. Chem. 277, 28853–28860.
[3] Selvaraj, A. and Prywes, R. (2003) Megakaryoblastic leukemia-1/2, a transcriptional co-activator of serum response factor, is required for skeletal myogenic differentiation. J. Biol. Chem. 278, 41977–41987.
[4] Cen, B., Salvaraj, A. and Prywes, R. (2004) Myocardin/MKL family of SRF coactivator: key regulators of immediate early and muscle specific gene expression. J. Cell Biochem. 93, 74–82.
[5] Pipes, G.C., Creemers, E.E. and Olson, E.N. (2006) The myocardin family of transcriptional coactivators: versatile regulators of cell growth, migration and myogenesis. Genes Dev. 20, 1545–1556.
[6] Miralles, F., Posern, G., Zaromytidou, A.I. and Treisman, R. (2003) Actin dynamics control SRF activity by regulation of its coactivator MAL. Cell 113, 329–342.
[7] Posern, G., Miralles, F., Guettler, S. and Treisman, R. (2004) Mutant actins that stabilize F-actin use distinct mechamisms to activate the SRF coactivator MAL. Embo J 23, 3973–3983.
[8] Vartiainen, M.K., Guettler, S., Larijani, B. and Treisman, R. (2007) Nuclear actin regulates dynamis subcellular localization and activity of the SRF cofactor MAL. Science 316, 1749–1752.
[9] Tabuchi, A., Estevez, M., Henderson, J.A., Marx, R., Shiota, J., Nakano, H. et al. (2005) Nuclear translocation of the SRF co-activator MAL in cortical neurons: role of RhoA signaling. J. Neurochem. 94, 169–180.
[10] Kalita, K., Kharebava, G., Zheng, J.J. and Hetman, M. (2006) Role of Megakaryoblastic acute leukemia-1 in ERK1/2-dependent stimulation of serum response factor-driven transcription by BDNF or increased synaptic activity. J. Neurosci. 26, 10020–10032.
[11] Shiota, J., Ishikawa, M., Sakagami, H., Tsuda, M., Baraban, J.M. and Tabuchi, A. (2006) Developmental expression of the SRF co-activator MAL in brain: role in regulating dendritic morphology. J. Neurochem. 98, 1778–1788.
[12] Ishikawa, M., Nishijima, N., Shiota, J., Sakagami, H., Tsuchida, K., Mizukoshi, M. et al. (2010) Involvement of the SRF coactivator megakaryoblastic leukemia in the activin-regulated dendritic complexity of rat cortical neurons. J. Biol. Chem. 285, 32734–32743.
[13] Heinemeyer, T., Wingender, E., Reuter, I., Hermjakob, H., Kel, A.E., Kel, O.V. et al. (1998) Databases on transcriptional regulation: TRANSFAC, TRRD, and COMPEL. Nucleic Acids Res. 26, 364–370.
[14] Mouilleron, S., Langer, C.A., Guettler, S., McDonald, N.Q. and Treisman, R. (2011) Structure of a pentavalent G-actin MRTF-A complex reveals how G-actin controls nucleocytoplasmic shuttling of a transcriptional coactivator. Sci. Signal 4, ra40 .
[15] Stern, S., Debre, E., Stritt, C., Berger, J., Posern, G. and Knöll, B. (2009) A nuclear actin function regulates neuronal motility by serum response factor-dependent gene transcription. J. Neurosci 29, 4512–4518.
[16] Wang, D., Chang, P.S., Wang, Z., Sutherland, L., Richardson, J.A., Small, E. et al. (2001) Activation of cardiac gene expression by myocardin, a transcriptional cofactor fro serum response factor. Cell 105, 851–862.
[17] Creemers, E.E., Sutherland, L.B., Oh, J., Barbosa, A.C. and Olson, E.N. (2006) Coactivation of MEF2 by the SAP domain proteins myocardin and MASTR. Mol. Cell 23, 83–96.

Journal of Neurochemistry

JOURNAL OF NEUROCHEMISTRY | 2014 | 128 | 507–522 doi: 10.1111/jnc.12486

ORIGINAL ARTICLE

Spikar, a novel drebrin-binding protein, regulates the formation and stabilization of dendritic spines

Hiroyuki Yamazaki,* Nobuhiko Kojima,* Kenichi Kato,* Eiji Hirose,† Toshiharu Iwasaki,‡ Toshiyuki Mizui,* Hideto Takahashi,*,[1] Kenji Hanamura,* Reiko T. Roppongi,* Noriyuki Koibuchi,‡ Yuko Sekino,*,§ Nozomu Mori†,[2] and Tomoaki Shirao*

*Department of Neurobiology and Behavior, Gunma University Graduate School of Medicine, Maebashi, Japan

†National Center for Geriatrics and Gerontology, Obu, Japan

‡Integrative Physiology, Gunma University Graduate School of Medicine, Maebashi, Japan

§Division of Pharmacology, National Institute of Health Sciences, Tokyo, Japan

Abstract

Dendritic spines are small, actin-rich protrusions on dendrites, the development of which is fundamental for the formation of neural circuits. The actin cytoskeleton is central to dendritic spine morphogenesis. Drebrin is an actin-binding protein that is thought to initiate spine formation through a unique drebrin-actin complex at postsynaptic sites. However drebrin overexpression in neurons does not increase the final density of dendritic spines. In this study, we have identified and characterized a novel drebrin-binding protein, spikar. Spikar is localized in cell nuclei and dendritic spines, and accumulation of spikar in dendritic spines directly correlates with spine density. A reporter gene assay demonstrated that spikar acts as a transcriptional co-activator for nuclear receptors. We found that dendritic spine, but not nuclear, localization of spikar requires drebrin. RNA-interference knockdown and overexpression experiments demonstrated that extranuclear spikar regulates dendritic spine density by modulating *de novo* spine formation and retraction of existing spines. Unlike drebrin, spikar does not affect either the morphology or function of dendritic spines. These findings indicate that drebrin-mediated postsynaptic accumulation of spikar regulates spine density, but is not involved in regulation of spine morphology.

Keywords: dendritic spine, drebrin-binding protein, spine formation, transcriptional co-activator.

J. Neurochem. (2014) **128**, 507–522.

*Read the **Editorial Highlight** for this article on page 473.*

Neurons have numerous small, actin-rich protrusions called dendritic spines that receive the majority of excitatory inputs (Sala *et al.* 2008; Rochefort and Konnerth 2012). The formation of dendritic spines plays a pivotal role in the incorporation of neurons into neural circuits (Kwon and Sabatini 2011). It is widely accepted that dendritic filopodia are the precursors of dendritic spines and that the actin cytoskeleton is a central player in the morphological changes underlying dendritic spine formation (Ethell and Pasquale 2005; Sekino *et al.* 2007; Shirao and Gonzalez-Billault 2013).

Drebrin is an actin-binding protein that has been extensively studied. Drebrin bridges two actin protomers (Grintsevich *et al.* 2010) and induces structural and

Received July 25, 2013; revised manuscript received October 9, 2013; accepted October 10, 2013.

Address correspondence and reprint requests to Tomoaki Shirao, Department of Neurobiology and Behavior, Gunma University Graduate School of Medicine, 3-39-22 Showa-machi, Maebashi 371-8511, Japan. E-mail: tshirao@med.gunma-u.ac.jp.

[1]Present address: Institut de recherches cliniques de Montreal, Montreal, QC, Canada, H2W 1R7. [2]Present address: Department of Anatomy and Neurobiology, Nagasaki University School of Medicine, Nagasaki, Nagasaki 852-8523, Japan.

Abbreviations used: ADF-H domain, actin-depolymerizing factor homology domain; BSA, bovine serum albumin; DIV, days *in vitro*; DMEM, Dulbecco's modified Eagle medium; drebrinR, RNAi-resistant drebrin; ERα, estrogen receptor α; GR, glucocorticoid receptor; His^6-drebrin, His^6-tagged drebrin A; KD, knockdown; LUC, luciferase; mDsRED, monomeric DsRED; MEM, minimum essential medium; mEPSCs, miniature excitatory postsynaptic currents; mNLS, mutated NLS; NLS, nuclear localization sequence; PBS, phosphate-buffered saline; RNAi, RNA interference; $spikar^R$, RNAi-resistant spikar; T3, 3,3′,5-triiodo-L-thyronine; TRE, thyroid hormone response element; TRβ1, thyroid hormone receptor β1.

mechanical remodeling of *F*-actin that includes significant changes in filament helical twisting and stiffness (Sharma *et al.* 2011, 2012). Within cultured cells, overexpressed drebrin binds to *F*-actin (Shirao *et al.* 1988; Ishikawa *et al.* 1994) to form unique *F*-actin bundles that are different from those observed in stress fibers or lamellipodia (Shirao *et al.* 1994). Formation of a drebrin-actin complex at postsynaptic sites during development facilitates dendritic spine formation (Takahashi *et al.* 2003; Aoki *et al.* 2005). Drebrin knockdown decreases spine and filopodia densities (Takahashi *et al.* 2006) and the density of excitatory synapses (Ivanov *et al.* 2009). However, drebrin overexpression does not increase the number of normal spines (Hayashi and Shirao 1999; Mizui *et al.* 2005), even though it causes morphological changes in dendritic spines (Hayashi and Shirao 1999; Biou *et al.* 2008). These results indicate that drebrin initiates spine formation, but an increased amount of drebrin does not directly correlate with the final density of dendritic spines.

We postulated the existence of a novel drebrin-binding protein that plays a critical role in regulating spine density through changes in its expression level. Although drebrin forms a complex with actin, myosin, and gelsolin (Hayashi *et al.* 1996) as well as other drebrin-binding proteins such as Homer2 (Shiraishi *et al.* 2004) and profilin (Mammoto *et al.* 1998), spine density does not vary in direct proportion to the expression level of these molecules (Sala *et al.* 2003; Ryu *et al.* 2006; Gorlich *et al.* 2012). To identify a drebrin-binding molecule directly related to spine density, we performed a yeast two-hybrid screen using drebrin as bait. Based on the screen results, we isolated a novel drebrin-binding protein that we termed spikar (for **spi**ne and **kar**yoplasm protein). Knockdown and overexpression experiments performed with spikar indicated that its expression level parallels the density of dendritic spines.

Methods

Animals

All experiments were carried out in accordance with the guidelines of the Animal Care and Experimentation Committee, Gunma University, Showa Campus (Maebashi, Japan). Wistar rats were purchased from Japan SLC Inc. (Hamamatsu, Japan) and Charles River Laboratories Japan Inc. (Yokohama, Japan). Every effort was made to minimize animal suffering and reduce the number of animals used. Animals were kept in the animal house under standard white cyclic lighting, with free access to food and water.

Yeast two-hybrid system

The *Saccharomyces cerevisiae* transformation and two-hybrid screen were carried out using the Y190 strain. The N-terminal region of rat drebrin (corresponding to amino acid residues 1–233) was subcloned into the pAS404 vector, which was derived from pAS1 (Sekiguchi *et al.* 2001). Y190 cells were transformed with the bait plasmid pAS404-drebrin (1–233), using the conventional lithium acetate-polyethylene glycol method. The cells were grown on SD medium lacking tryptophan and further characterized by testing for protein expression and self-activation of the bait before screening. Large-scale transformation was performed using a rat brain cDNA library constructed in a pACT2 vector (Clontech, Palo Alto, CA, USA), and the cells were grown on SD medium lacking tryptophan, leucine, and histidine, and containing 25 mM 3-aminotriazole. The cells were subsequently assayed for activation of the HIS3 genes.

Molecular cloning of spikar cDNA

The rat spikar clone isolated from the two-hybrid screen lacked a 5′-coding sequence; therefore, the full-length cDNA was generated using a PCR-based strategy. To obtain the 5′ end of rat spikar cDNA, we performed 5′-rapid amplification of cDNA ends (RACE) using rat hippocampal cDNA and a 5′-Full RACE Core Set (Takara, Otsu, Japan).

Expression vectors

All spikar and drebrin constructs were generated by PCR using Pfu turbo DNA polymerase (Stratagene, La Jolla, CA, USA). Full-length spikar and its deletion mutants were subcloned into pEGFP-C1 (EGFP, enhanced green fluorescent protein) (Clontech), pCMV-Myc (Clontech) or pNN265-HA (Kojima *et al.* 1997). To generate the nuclear localization signal (NLS) mutant of spikar (mNLS-spikar), K44T and K45T mutations were introduced by PCR using the following primers: 5′-gccccattaaaacgacaaagaaacccggc-3′ and 5′-gccgggtttctttgtcgttttaatggggc-3′.monomeric DsRED-drebrin A was constructed by subcloning a rat drebrin A fragment into the pDsRed-Monomer-C1 (Clontech).

Reporter gene assays

The method of reporter gene assay has been described previously (Takeshita *et al.* 1998; Iwasaki *et al.* 2001, 2002). The details are provided in the Appendix S1.

In vitro binding assay

A binding assay for full-length drebrin and full-length spikar was performed using green fluorescent protein (GFP)-spikar and His^6-tagged drebrin A (His^6-drebrin). The His^6-drebrin construct was a gift from Dr Ishikawa (Ishikawa *et al.* 2007). His^6-drebrin was affinity purified using Ni-NTA Magnetic Agarose Beads (Qiagen, Hilden, Germany). Ni-NTA beads conjugated with His^6-drebrin were incubated with cell lysate expressing GFP-spikar for 2 h at 25°C. Following extensive washes with lysis buffer (20 mM Tris-HCl, pH 7.5, 150 mM NaCl, 1% NP40, 50 μg/mL DNase, 10 μg/mL RNase, 1 mM phenylmethanesulfonyl fluoride, 1 μg/mL leupeptin, and 1 μg/mL pepstatin), the Ni-NTA bead pellets were re-suspended in sodium dodecyl sulfate (SDS) sample buffer and analyzed by western blotting. For GST pull-down assay, Glutathione S-transferase (GST)-drebrin (1–138) (pGEX-4T-1, GE Health Care, Buckinghamshire, England) was purified directly from bacterial extracts on glutathione-Sepharose-4B (GE Health Care). Immobilized GST or GST-drebrin (1–138) fusion proteins were incubated with cell lysate expressing HA-spikar fragments (1–376, 377–1208, or 1–1208) for 2 h at 25°C. After extensive washes with lysis buffer, the GST bead pellets were re-suspended in SDS sample buffer and analyzed by western blotting.

Immunocytochemistry and immunohistochemistry

Cultured neurons were fixed in 4% paraformaldehyde at 4°C for 20 min. The fixed neurons were permeabilized with 0.1% Triton X-100 in phosphate-buffered saline (PBS) for 5 min and blocked with 3% bovine serum albumin (BSA) in PBS for 60 min. Primary antibodies were applied in 3% BSA/PBS at 4°C for 12 h. After washing with PBS three times for 5 min each, the appropriate secondary antibodies conjugated to fluorescein isothiocyanate, Cy5, or rhodamine (Chemicon, Temecula, CA, USA) were added and incubated for 1 h at 20–25°C.

Deeply anesthetized 7-week-old male Wistar rats were perfused intracardially with a fixative of 4% paraformaldehyde in 0.1 M phosphate buffer (pH 7.4). Brain tissue was post-fixed in the same fixative for 12 h and then equilibrated with 30% sucrose in PBS at 4°C. Frozen sections (25 μm) were cut on a cryostat and treated with 0.1% Triton X-100 in PBS for 10 min and then incubated with 3% BSA/PBS for 1 h. They were then incubated with the primary antibody for 12 h at 4°C, washed with PBS four times for 5 min each, incubated with a biotinylated secondary antibody (Vector Laboratories, Burlingame, CA, USA) for 1 h at 20–25°C, and washed four times for 5 min each. Visualization was performed with 3,3′-diaminobenzidine using the ABC method (Vectastain Elite kit, Vector Laboratories).

Western blot analysis and subcellular fractionation

Wistar rats were sacrificed after being deeply anesthetized, and various tissues were dissected and homogenized. Protein amounts were normalized to the wet weights of the original tissue samples. For subcellular fractionation, the cerebral cortices of seven adult male Wistar rats were homogenized in a buffered solution (320 mM sucrose, 4 mM HEPES-NaOH, pH 7.4) containing a protease inhibitor cocktail (Complete, Roche, Basel, Switzerland) and fractionated according to the method of Huttner *et al.* (1983). For extraction experiments, the P3 pellet was homogenized by a Teflon homogenizer in a buffer solution containing 1 M NaCl or 1% Triton X-100 and centrifuged at 165 000 *g*. The samples were denatured and subjected to SDS–polyacrylamide gel electrophoresis. The proteins were then transferred onto an Immobilon Transfer Membrane (Millipore, Bedford, MA, USA) and processed for immunodetection.

Antibodies

The following primary antibodies were used: mouse monoclonal anti-drebrin (M2F6; Shirao and Obata 1986), mouse monoclonal anti-PSD-95 (7E3-1B8; Affinity BioReagents, Golden, CO, USA), mouse monoclonal anti-MAP2 (HM-2; Sigma, St. Louis, MO, USA), mouse monoclonal anti-Glial fibrillary acidic protein (anti-GFAP) (G-A-5; Sigma) and rabbit polyclonal anti-synapsin I (Chemicon). Polyclonal anti-spikar antibodies were raised against the C-terminal region of spikar (377–1208). The DNA fragment of spikar (377–1208) was subcloned into pET19b (Novagen, Madison, WI, USA). His^6-spikar (377–1208) was affinity-purified using a Ni^{2+} column (GE Health Care) according to the manufacturer's instructions. This His^6-spikar (377–1208) protein (2 mg) was used to immunize rabbits. The specificity of the anti-spikar antibodies was confirmed by western blotting (Figure S1).

Cell culture and transfection

Hippocampi were dissected from the fetuses of timed pregnant Wistar rats at embryonic day 18. The hippocampi were trypsinized and dissociated by trituration according to methods described previously (Takahashi *et al.* 2003). Briefly, cell suspensions were plated at a density of 5000 cells/cm^2 on coverslips coated with poly-L-lysine and incubated in minimum essential medium (Invitrogen) supplemented with 10% fetal bovine serum. Following cell attachment, the coverslips were transferred to a culture dish containing a glial monolayer sheet and maintained in serum-free minimum essential medium with B27 supplement (Invitrogen). Cytosine β-D-arabinofuranoside (10 μM; Sigma) was added to the cultures at 4 days *in vitro* (DIV) to inhibit glial proliferation.

Cells were transfected using the CaPO4 method (Details are provided in Figure S2). Microinjection was performed using a micromanipulator 5171 (Eppendorf, Hamburg, Germany).

HEK293 cells were cultured in Dulbecco's modified Eagle medium supplemented with 10% fetal bovine serum at 37°C in a 5% CO_2 atmosphere. Cells were transfected using Lipofectamine 2000 (Invitrogen).

RNA interference

To generate the RNA interference (RNAi) constructs used in this study, the following DNA oligonucleotides were annealed and subcloned into the pSUPERneo+GFP vector (OligoEngine, Seattle, WA, USA): 5′-gatccccggatcagttagagttaggattcaagagatcttagctctgactg atccttttggaaa-3′ and 5′-agcttttccaaaaaggatcagtcagagctaagatctcttgaatc ctaactctaactgatccggg-3′ (Spikar-shRNA-2); 5′-gatccccgttgatgcaagtag cagagttcaagagactttgctatttgcgtcaacttttggaaa-3′ and 5′-agcttttccaaaaagt tgacgcaaatagcaaagtctcttgaactctgctacttgcatcaacggg-3′ (Spikar-shRNA -3); 5′-gatccccgtgatgtgtggtttctgtattcaagagatgcagaaaccgtacatcac tttttg gaaa-3′ and 5′-agcttttccaaaaagtgatgtacggtttctgcatctcttgaata cagaaacc acacatcacggg-3′ (Drebrin-shRNA); 5′-gatccccccttacgttgagtacttcggttca agagatcgaagtactcagcgtaagttttta-3′ and 5′-agcttaaaaac ttacgctgagtact tcgatctcttgaaccgaagtactcaacgtaagggg3′ (Luciferase-shRNA). The targeted regions were not homologous to any other known genes, as confirmed by a BLAST search. The RNAi-resistant mutant of spikar-shRNA-3 was constructed by PCR using the following primers: 5′-ccacaagttgacgcagatcgcaaaggttgtcatc-3′ and 5′-gat-gacaacctttgcgatctgcgtcaacttgtgg-3′. The RNAi-resistant mutant of drebrin was constructed by PCR using the following primers: 5′-gaaagtgatgtatggcttctgcagcgtc-3′ and 5′- gacgctgcagaagccatacatca ctttc-3′. A spikar-shRNA-3 construct was used to silence spikar. Cultured hippocampal neurons were transfected at 3 DIV with spikar-shRNA-3 to ensure that spikar expression would be suppressed during stage 5 of neuronal development (Dotti *et al.* 1988). Empty shRNA vector (pSUPERneo+GFP) was used as a control. The effect of the control vector on dendritic protrusions was similar to that of luciferase-shRNA vector (Figure S2). Another effective construct, spikar-shRNA-2, showed a reduction of the density of dendritic spines and filopodia similar to spikar-shRNA-3 (Figure S2). The efficiency of the drebrin knockdown construct has been described previously (Kato *et al.* 2012).

Electrophysiology

Whole-cell patch clamp recordings were performed with an Axopatch 200A amplifier (Axon Instruments, Union City, CA, USA) at 20–25°C. GFP-positive cultured hippocampal neurons from

17–19 DIV were identified using fluorescence microscopy (Olympus IX70, Tokyo, Japan) and used for electrophysiological studies. Patch pipettes were made from borosilicate glass capillaries (1.5 mm OD; Narishige, Tokyo, Japan) using a micropipette puller (P-87; Sutter Instrument, Novato, CA, USA). The resistance of the patch pipettes was 3–4 MΩ when filled with the pipette solution described below. The series resistance, 9.8 ± 0.6 MΩ, was not electronically compensated. The reference electrode was an Ag/AgCl electrode connected to the bath via an agar bridge filled with 150 mM NaCl. The potential of the pipette was corrected for the measured liquid junction potential (approximately 10 mV). Modified Tyrode solution was used as the external solution containing (in mM) 145 NaCl, 5 KCl, 2 $CaCl_2$, 1 $MgCl_2$, 10 glucose, and 10 HEPES (pH 7.4 with NaOH) plus 1 μM tetrodotoxin and 100 μM picrotoxin. The pipette solution contained (in mM) 122.5 Cs-gluconate, 17.5 CsCl, 8 NaCl, 0.2 EGTA, 2 ATP-Mg, 0.3 GTP, and 10 HEPES, and the pH was adjusted to 7.2 with Cs-OH. Whole-cell currents were recorded at 10 kHz after low-pass filtering at 2 kHz, and miniature excitatory postsynaptic currents (mEPSCs) were analyzed offline using Mini Analysis Software (Synaptosoft Inc., Decatur, GA, USA). We held the membrane potential of cultured neurons at −60 mV in voltage clamp and recorded the synaptic current.

Image analysis and statistics

Fluorescence images were acquired using a Zeiss Axioplan 2 microscope (Carl Zeiss, Jena, Germany) equipped with a CoolSnap fx CCD camera (Photometrics, Tucson, AZ, USA) and a 63 × oil-immersion, 1.4 NA (Carl Zeiss) objective at 25°C. The data were collected from two to three independent culture preparations, and analysis was performed by an experimenter blinded to the identity of the transfected constructs. Morphometric analysis and quantification were carried out using MetaMorph image analysis software (Molecular Devices, Sunnyvale, CA, USA). Neurons expressing GFP were imaged and quantified, and aspiny interneurons were excluded from the analysis. For each neuron, one or two dendrites 40–80 μm from the first branching point were selected and analyzed. For the morphological analysis of the dendritic protrusions, the maximum length and width of each protrusion of length 0.5–8 μm were measured manually (Figure S3a and b). Dendritic spines were defined as dendritic protrusions with a head or stubby type protrusion for which the length:width ratio was less than or equal to 2. Dendritic filopodia were defined as headless dendritic protrusions for which the length:width ratio was greater than 2. For the quantification of cluster number, clusters were defined as an immunostained region with a peak fluorescence level that was 2-fold greater than the averaged fluorescence level of the dendrites. For image analysis, statistical significance was determined with a Welch's *t*-test, Mann–Whitney U-test, Dunnett multiple comparison test, Tukey–Kramer multiple comparison test or Steel–Dwass multiple comparison test. Spine length and width were analyzed with the Kolmogorov–Smirnov test using SPSS software (SPSS, Chicago, IL, USA). p values less than 0.01 were considered statistically significant unless explicitly stated otherwise. For electrophysiology, statistical significance was determined with a Welch's *t*-test. Cumulative frequencies of mEPSC amplitude and inter-event interval were analyzed with the Kolmogorov–Smirnov test using Mini Analysis Software (Synaptosoft, Inc., NJ, USA). For reporter gene assays, all transfection studies were repeated at least twice in triplicate. Statistical analysis was performed using ANOVA followed by a post hoc comparison with Bonferroni's multiple range test. The data shown represent the mean values of triplicate transfections ± SEM.

Live-cell imaging

Live neurons were mounted in a modified 35-mm dish and imaged with a 40 × , 0.75 NA water-immersion objective (Carl Zeiss) in culture medium using the microscope described above. The images were captured within 5 min at 30°C.

Results

Spikar is a novel drebrin-binding transcriptional co-activator

To identify proteins that interact with drebrin, we performed a yeast two-hybrid screen using a rat brain cDNA library. We used the N-terminal region of drebrin (amino acids 1–233), which contains the actin-depolymerizing factor homology domain (ADF-H domain), as the screen bait. In the course of screening approximately 9×10^7 colonies, we isolated 89 independent clones. DNA sequencing of these clones showed that 64 of the 89 clones encoded the same protein. We termed this protein spikar (accession number AB074010); this name was derived from its unique subcellular localization (in spines and nuclei), as described in the following section. A computational analysis using the NCBI database indicated that spikar was a rat ortholog of human KIAA1125 (accession number AB032951) and human prkcbp1 (accession number AF233453) (Fossey *et al.* 2000), and that rat spikar could be further classified into three isoforms: spikar A (isolated in this study, accession number AB074010), spikar B (XP_215942), and spikar delta-C (isolated in this study, AB721962) (Fig. 1a). Spikar contains a NLS, Plant Homeo Domain, Bromo domain, nuclear receptor recognition sequence (a LXXLL motif), PWWP domain, coiled-coil domain, and a MYND domain (Fig. 1a). In the following experiments, we used spikar A unless explicitly stated otherwise.

BS69 is a spikar-like protein containing Plant Homeo Domain, Bromo, PWWP, coiled-coil, and MYND domains (Fig. 1a), and is a co-repressor of transcription (Masselink and Bernards 2000). Because spikar has a domain structure similar to BS69, we used a reporter gene assay to examine whether spikar affects transcription in the kidney fibroblast cell line CV1. When spikar was co-transfected with thyroid hormone receptor β1 (TRβ1), spikar potentiated TRβ1-mediated transcription of thyroid hormone response element in the presence of its ligand, triiodothyronine (T3; Fig. 1b). This activation was induced by T3 and was dependent on the spikar dose, indicating that spikar is a transcriptional co-activator for TRβ1 activity. This co-activator activity of

spikar was also detected in the neuroblastoma cell line N2A (Fig. 1c). In addition, spikar activated transcription mediated by the glucocorticoid receptor and estrogen receptor α (Figure S4a and b), both of which are expressed in the hippocampus (Tohgi *et al.* 1995). These data suggest that spikar acts as a transcriptional co-activator for nuclear receptors in these cells.

Spikar and drebrin interact at their N-terminal regions

We examined whether full-length drebrin binds to full-length spikar using a pull-down assay. His^6-drebrin specifically pulled down GFP-spikar from lysates of cells expressing GFP-spikar (Fig. 1d), demonstrating that drebrin can bind to spikar *in vitro*.

Next, we identified the spikar-binding region of drebrin using a yeast two-hybrid assay with drebrin (1–134) and drebrin (135–233). This assay showed that drebrin (1–134) bound to spikar, but drebrin (135–233) did not (Figure S5a). We then constructed a series of deletion derivatives of spikar to determine which region is required for the interaction with drebrin (1–134). Spikar (88–376), which contains the N-terminal region of spikar, bound strongly to drebrin (1–134). In contrast, spikar (384–1208) did not bind to drebrin. Because spikar (88–258) showed no significant binding activity, and spikar (146–376) showed only weak binding activity (Figure S5b), it appears that spikar (88–376) is necessary for strong drebrin-binding activity. A pull-down assay also demonstrated that full length HA-spikar as well as HA-spikar (1–376) bound to GST-drebrin (1–138), but HA-spikar (377–1208) did not (Fig. 1e). These data were consistent with the results of the yeast two-hybrid assay.

Immunochemical analysis of spikar expression

Immunoblot analysis of protein extracts prepared from various adult rat tissues showed that spikar was ubiquitously detected in the brain, spinal cord, thymus, liver, kidney, spleen, lung, heart, and testis, although the expression levels varied among the tissues (Fig. 1f). Notably, spikar expression levels were high in the thymus and spleen. In the central nervous system, spikar expression was greater in the cerebellum than the cerebral cortex and the spinal cord; spikar was hardly detected in glial cultures (Fig. 1g).

We next examined the subcellular distribution of spikar in cerebral cortex homogenate. Spikar was recovered mainly in the P1 fraction, which includes the cell nuclei. A small amount of spikar was also recovered in the P3 (microsomal) fraction (Fig. 1h). Drebrin was also recovered in the P3 fraction. To characterize the association of spikar with the P3 fraction, we treated the P3 fraction with detergent or a high salt solution. Spikar was detected in the cytosolic fraction formed by treatment with a high concentration of salt (1 M NaCl), whereas only faint amounts were detected in the cytosolic fraction formed by treatment with 1% Triton X-100 (Fig. 1i). As an internal control for membrane protein, we used an immunoglobulin binding protein (Bip), which was solubilized by 1% Triton X-100 but not by 1 M NaCl. These results indicate that spikar was recovered in the P3 fraction owing to protein–protein, but not protein–membrane, interactions.

Localization of spikar in neuronal nuclei and dendritic spines

Although spikar immunostaining was observed in most brain regions, intense immunostaining was particularly observed in regions with high cellular densities, such as the granule cell and pyramidal layers of the hippocampus and the granular layer of the cerebellum (Fig. 2a). Higher magnification images showed that spikar immunostaining was observed in cell nuclei as well as in a punctate staining pattern along dendrites (Fig. 2b and c).

Similarly, immunocytochemical analysis of hippocampal neurons cultured for 21 DIV showed that spikar immunostaining was present in cell nuclei and distributed along dendrites in a punctate pattern (Fig. 2d, left panels). Spikar immunopositive puncta were also stained with antibodies against drebrin (Fig. 2d, right panels). In the dendritic shaft of developing neurons, spikar was localized mainly in dendritic shaft at DIV 7 but in dendritic spines at DIV 14 (Figure S6). Furthermore, GFP-spikar expressed in cultured neurons accumulated in the nuclei and co-localized with drebrin (Fig. 2e). Because these data indicated that spikar is present in the spine and karyoplasm, we named the protein spikar.

Spikar knockdown decreases spine density during development

We next analyzed the role of spikar in dendritic spine formation. To reduce the expression of spikar, we used two short hairpin RNAs (shRNAs; pSUPER-RNAi-2 and -3) that targeted different regions of spikar mRNA. Both effectively suppressed the exogenous expression of myc-spikar in HEK293 cells (Fig. 3a). In cultured hippocampal neurons, the immunofluorescence intensity of endogenous spikar in the nucleus was decreased to 20% of control by 96 h after transfection with pSUPER-RNAi-3 (spikar-shRNA-3; Fig. 3b and c).

We knocked down spikar at 3 DIV and analyzed the effect on morphogenesis of dendritic protrusions at 16 DIV. We selected transfected neurons by GFP expression. Neuronal morphology was visualized by GFP fluorescence (Fig. 3d). Spikar knockdown (KD) caused a significant decrease in the density of dendritic spines and filopodia at 16 DIV (Control: 43.7 ± 1.8 spines/100 μm; 19.4 ± 1.2 filopodia/100 μm; Spikar KD: 20.6 ± 1.1 spines/100 μm; 11.6 ± 0.9 filopodia/100 μm; $*p < 0.01$; Fig. 3e–g). Interestingly, cumulative frequency distributions showed no differences between the lengths and widths of dendritic spines in spikar-KD and control neurons (Fig. 3h, i), indicating that spikar KD does not affect spine morphology.

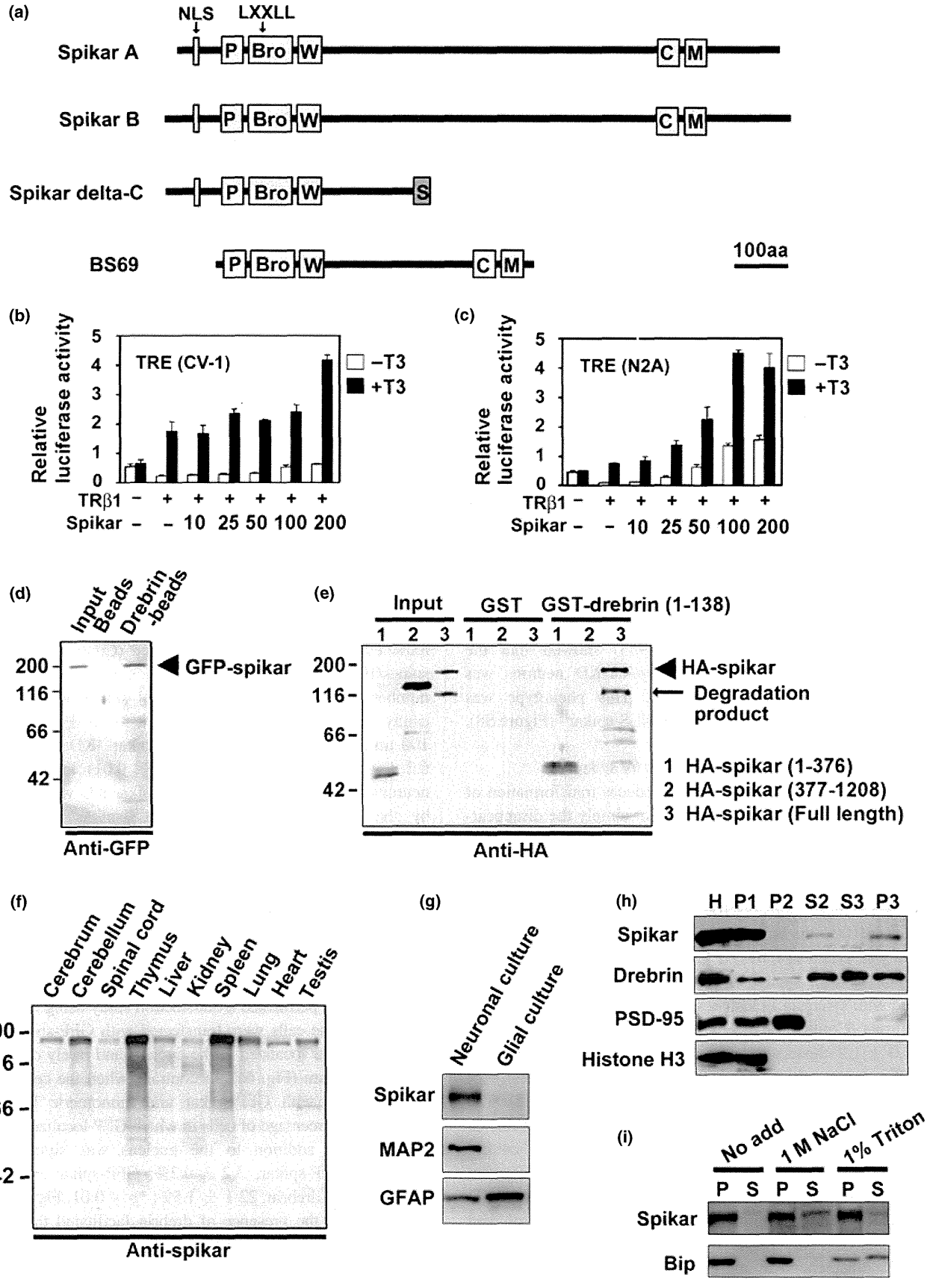
(a)
NLS
LXXLL
Spikar A
Spikar B
Spikar delta-C
BS69
P
Bro
W
C
M
S
100aa
(b)
TRE (CV-1)
Relative luciferase activity
−T3
+T3
TRβ1 − + + + + + +
Spikar − − 10 25 50 100 200
(c)
TRE (N2A)
Relative luciferase activity
−T3
+T3
TRβ1 − + + + + + +
Spikar − − 10 25 50 100 200
(d)
Input
Beads
Drebrin -beads
200
116
66
42
GFP-spikar
Anti-GFP
(e)
Input
GST
GST-drebrin (1-138)
1 2 3 1 2 3 1 2 3
200
116
66
42
HA-spikar
Degradation product
1 HA-spikar (1-376)
2 HA-spikar (377-1208)
3 HA-spikar (Full length)
Anti-HA
(f)
Cerebrum
Cerebellum
Spinal cord
Thymus
Liver
Kidney
Spleen
Lung
Heart
Testis
200
116
66
42
Anti-spikar
(g)
Neuronal culture
Glial culture
Spikar
MAP2
GFAP
(h)
H P1 P2 S2 S3 P3
Spikar
Drebrin
PSD-95
Histone H3
(i)
No add
1 M NaCl
1% Triton
P S P S P S
Spikar
Bip

Fig. 1 Characterization of spikar. (a) Schematic diagram of domain structures of spikar isoforms and BS69. P, Plant Homeo Domain (PHD) domain; Bro, Bromo domain; W, PWWP domain; C, Coiled-coil; M, MYND domain. (b, c) Spikar-activated nuclear-receptor-mediated transcription in CV-1 (b) and N2A cells (c). Cells were grown in the presence or absence of T3 (100 nM). (d) *In vitro* binding assay for the interaction between drebrin and spikar. Input: cell lysate containing GFP-spikar; Beads: samples precipitated with Ni-NTA beads; Drebrin-beads: samples precipitated with drebrin-conjugated beads. (e) GST pull-down assay for spikar and drebrin. Lysates of cells expressing each HA-spikar fragment (1, 1–376; 2, 377–1208; 3, 1–1208) were pulled down with GST-drebrin (1–134). (f) Western blotting of extracts from various tissues (200 μg wet weight for each). (g) Western blotting of lysates (5 μg protein) from neural and glial cultures. (h) Subcellular distribution of spikar. The protein extract (20 μg protein) from each fraction was analyzed by western blotting. H, homogenate; P1, cell nuclei and debris; P2, synaptosomal fraction; S2, non-synaptosomal fraction; S3, cytosolic fraction; P3, microsomal fraction. (i) The P3 fraction from rat cerebral cortices was treated with 1 M NaCl or 1% Triton X-100. The insoluble pellet (P) and supernatant (S) were analyzed by western blotting.

To assess the specificity of the effect of spikar KD on spine density, we performed a rescue experiment using RNAi-resistant spikar (myc-spikar^R), which is distributed to both the cytoplasm and nucleus (Figure S7a), or RNAi-resistant spikar with a mutated nuclear localization sequence (myc-mNLS-spikar^R), which does not enter the nucleus (Figure S7b). Expression of myc-spikar^R significantly increased the density of dendritic spines and filopodia (31.5 ± 1.0 spines/100 μm; 23.2 ± 0.8 filopodia/100 μm; $*p < 0.01$ vs. Spikar KD, Fig. 5e–g) of spikar-KD neurons. Expression of myc-mNLS-spikar^R also rescued the decrease in spine and filopodia densities (30.2 ± 1.1 spines/100 μm; 20.0 ± 0.8 filopodia/100 μm; $*p < 0.01$ vs. Spikar KD, Fig. 5e–g). In addition, we analyzed the dendritic arborization of spikar-KD neurons. Sholl analysis (Sholl 1953) showed that the arborization of the dendrites of spikar-KD neurons was significantly reduced (Figure S8). This phenotype was rescued by cotransfection of myc-mNLS-spikar^R (Figure S8).

Spikar knockdown decreases excitatory synapses

We examined whether spikar KD induces transformation of spine synapses into shaft synapses, or simply the disappearance of spine synapses. Immunocytochemical analysis showed that both PSD-95 and synapsin I clusters were significantly reduced in spikar-KD neurons (Control: PSD-95, 78.1 ± 4.3 clusters/100 μm; synapsin I, 125.4 ± 4.2 clusters/100 μm; Spikar KD: PSD-95, 50.0 ± 2.2 clusters/100 μm; synapsin I, 81.1 ± 2.9 clusters/100 μm; $*p < 0.01$, Fig. 4a and b). Synaptic PSD-95 clusters that were co-localized with synapsin I clusters were also reduced in spikar-KD neurons (Control, 63.0 ± 4.2 clusters/100 μm; Spikar KD, 34.0 ± 1.9 clusters/100 μm; $*p < 0.01$, Fig. 4b, right).

We next analyzed the spontaneous synaptic activity of spikar-KD neurons using electrophysiology (Fig. 4c). The amplitude of mEPSCs in spikar-KD neurons was 20.1 ± 2.0 pA, which was similar to that observed in control neurons (19.1 ± 2.3 pA; Fig. 4d). However, the inter-event interval of mEPSCs was significantly longer in spikar-KD neurons than in control neurons (568.8 ± 98.8 ms and 320.7 ± 63.5 ms, respectively, $p < 0.05$; Fig. 4e). These immunohistochemical and electrophysiological data indicate that spikar KD decreases the density of excitatory synapses, and suggest that spikar regulates the dendritic spine density with a concomitant change in the density of excitatory synapses.

Spikar knockdown facilitates the retraction of existing spines and suppresses the addition of new spines

To analyze whether spikar functions in spine stabilization or *de novo* spine formation, we followed the fate of spines using live-cell imaging (Fig. 5a). Cultured hippocampal neurons were transfected at 8 DIV with spikar-KD vector, and the same cells were analyzed at 16 and 22 DIV (a mature stage of cultured neurons) by imaging GFP fluorescence (Fig. 5b). During the 6-day period from 16 to 22 DIV, the number of retracted spines significantly increased (Control, 9.1 ± 1.0 spines/100 μm; Spikar KD, 15.5 ± 1.3; $*p < 0.01$), and the numbers of persistent and additional spines were significantly decreased (Control: persistent, 15.3 ± 0.9 spines/100 μm; addition, 20.5 ± 2.1; Spikar KD: persistent, 6.2 ± 1.6; addition, 4.2 ± 0.7; $*P < 0.01$) in spikar-KD neurons (Fig. 5c). These effects of spikar KD were blocked by the co-expression of myc-mNLS-spikar^R (retraction, 7.8 ± 0.7 spines/100 μm; persistent, 15.2 ± 1.2; addition, 18.9 ± 1.4; $*P < 0.01$ vs. Spikar KD, Fig. 5c). These results indicate that extranuclear spikar is required for the *de novo* formation and stabilization of dendritic spines.

Localization of spikar in dendritic spines depends on drebrin

To test whether the subcellular localization of spikar depends on drebrin, we performed a transfection study using HEK293 cells. When the cells were transfected with GFP-spikar, the GFP signal was localized to the nucleus and rarely observed in the cytoplasm (Fig. 6a). In contrast, when the cells were co-transfected with GFP-spikar and monomeric DsRED-drebrin, the percentage of cells in which GFP localized to the cytoplasm in addition to the nucleus was significantly increased (GFP-spikar, 3.2 ± 0.2%; GFP-spikar + monomeric DsRED-drebrin, 22.1 ± 1.5%; $*p < 0.01$, Fig. 6b and c). Therefore, the presence of drebrin facilitated the extranuclear distribution of spikar within the cells, suggesting that drebrin anchors spikar within the cytoplasm. When we

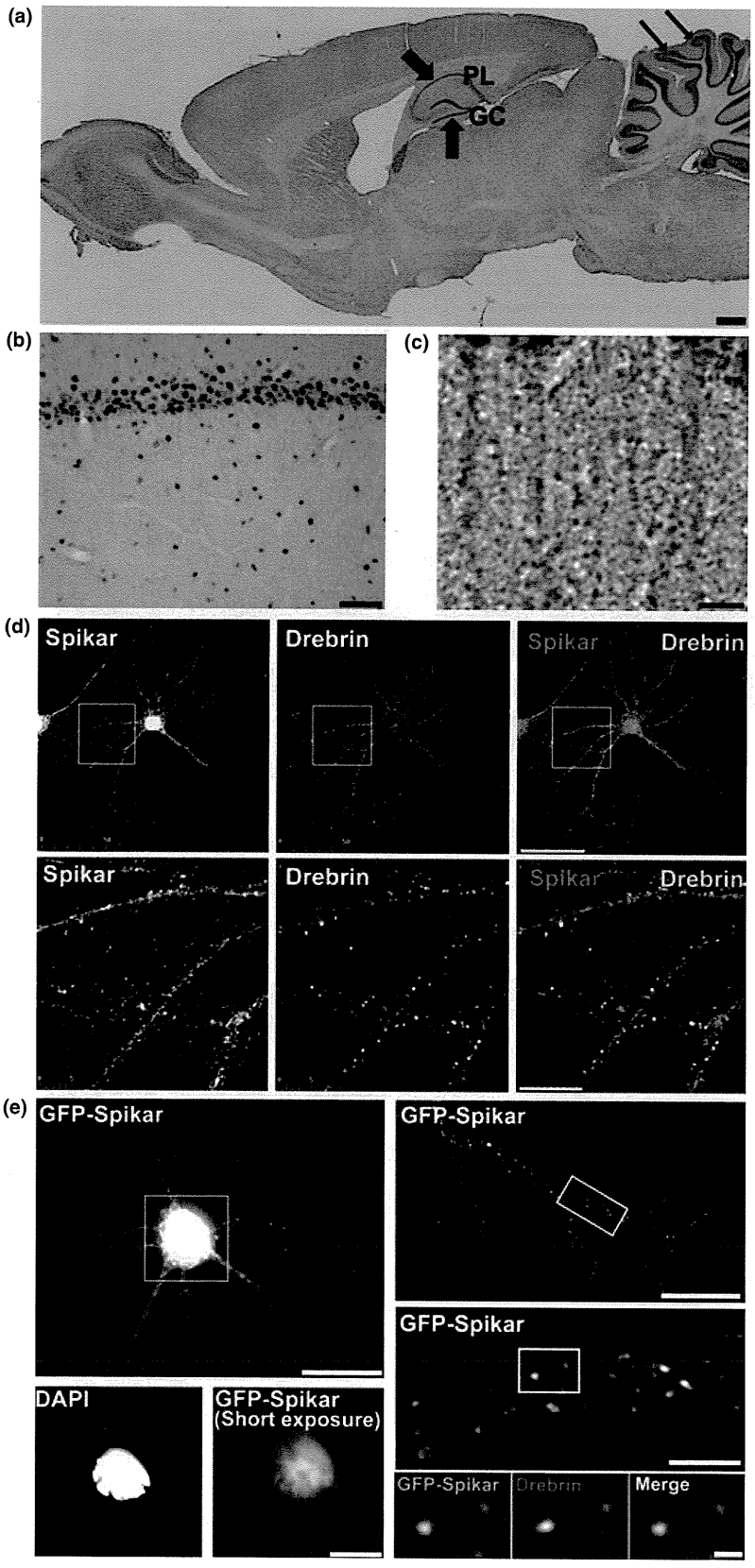

Fig. 2 Spikar is localized in neuronal nuclei and dendritic spines. (a–c) Immunohistochemical staining for spikar in adult rat brain. (a) Low magnification images of sagittal sections. Large arrows indicate granule cell and pyramidal layers of the hippocampus. Small arrows show the granular layer of the cerebellum. Scale bar, 1 mm. (b) Coronal section of hippocampal CA1 region. Scale bar, 50 μm (c) Higher magnification view of pyramidal neurons of the hippocampus. Note the punctate staining pattern observed in the dendritic region. Scale bar, 5 μm. (d) Cultured neurons were immunostained with spikar and drebrin antibodies at 21 DIV. The high magnification views (lower panels) show that spikar signals (red) overlap with drebrin signals (green) in dendritic spines. Scale bars, 50 μm (upper); 10 μm (lower). (e) Cultured neurons were microinjected with GFP-spikar at 21 DIV and analyzed at 22 DIV. Scale bars, 30 μm (upper); 5 μm (lower).

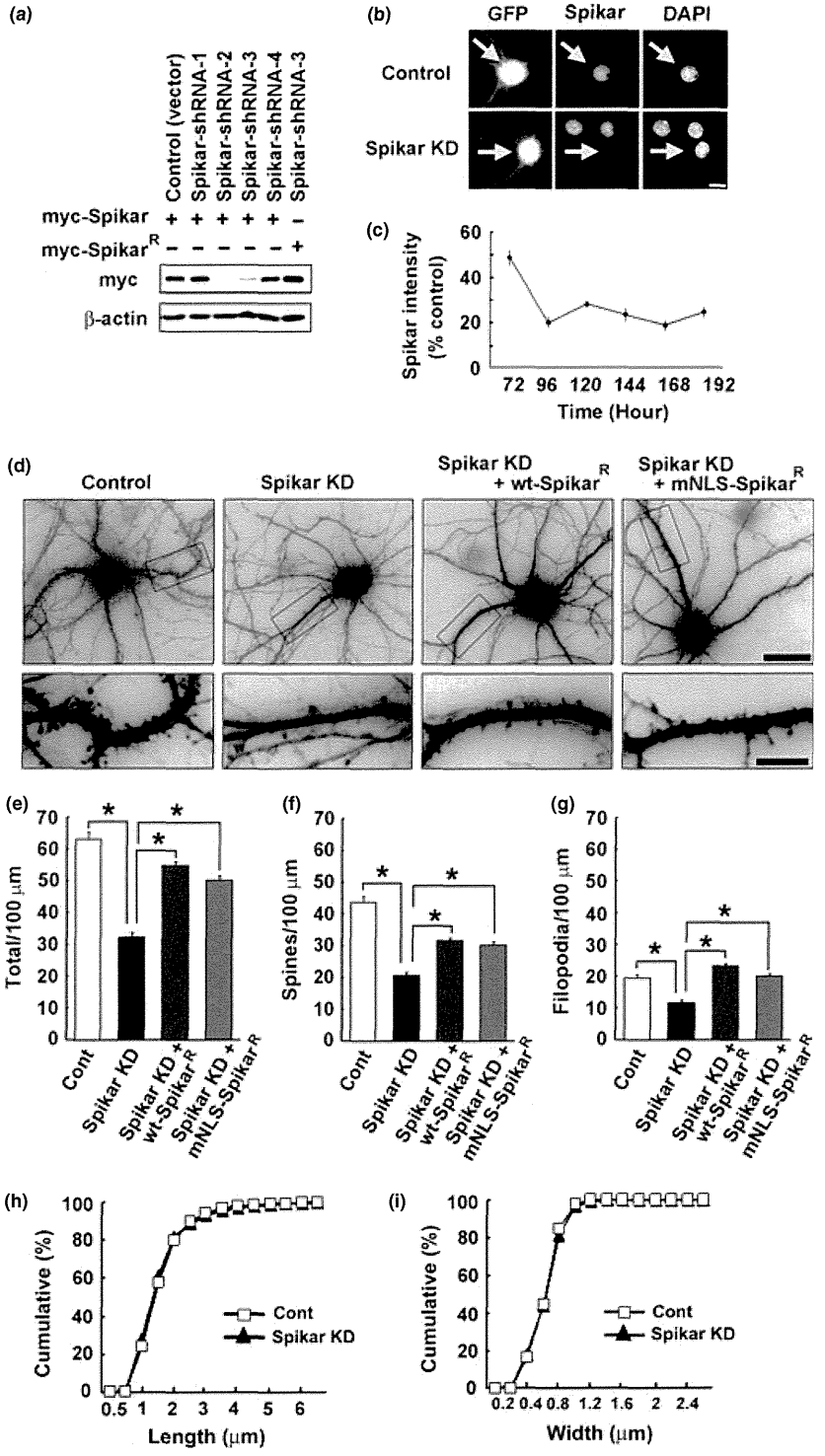

Fig. 3 Spikar knockdown reduces the density of dendritic spines and filopodia. (a) Efficacy of shRNAs. Note that myc-spikar^R is an RNAi-resistant mutant that is not affected by Spikar-shRNA-3. (b) Cultured hippocampal neurons were transfected with either an empty vector (control) or spikar-shRNA-3 and immunostained for spikar. Arrows indicate transfected neurons. Scale bar, 10 μm. (c) Timecourse of spikar knockdown (KD) in cultured hippocampal neurons. (d) Cultured neurons were transfected with an empty vector (cont), spikar-shRNA-3, spikar-shRNA-3+ myc-spikar^R, or spikar-shRNA-3+ myc-mutated nuclear localization sequence (mNLS)-spikar^R at 3 DIV and analyzed at 16 DIV. Scale bars, 30 μm (upper) and 10 μm (lower). (e–g) Quantification of effects of spikar KD on the density of total protrusions (spines and filopodia), spines, and filopodia. Data are presented as mean ± SEM ($n > 100$, $^*p < 0.01$, Tukey–Kramer test). (h, i) Cumulative frequency plots of the length and width of dendritic protrusions in neurons transfected with empty vector or spikar-shRNA-3. Data were collected from 1800–2500 protrusions from > 100 neurons for each group.

transfected myc-spikar into cultured hippocampal neurons, myc-spikar was localized to dendritic spines and the nucleus, similar to the expression pattern of endogenous spikar (Fig. 6d). In the dendritic spines, strong immunostaining of myc-spikar co-localized with strong drebrin signals. The immunofluorescence intensity of myc-spikar in the dendritic spines correlated with that of drebrin (correlation coefficient $r = 0.59$, $p < 0.01$, Fig. 6e).

Next, we examined whether drebrin KD changed the intracellular localization of myc-spikar in cultured neurons. We silenced the expression of drebrin using RNAi and then analyzed the localization of spikar. Myc-spikar was distrib-

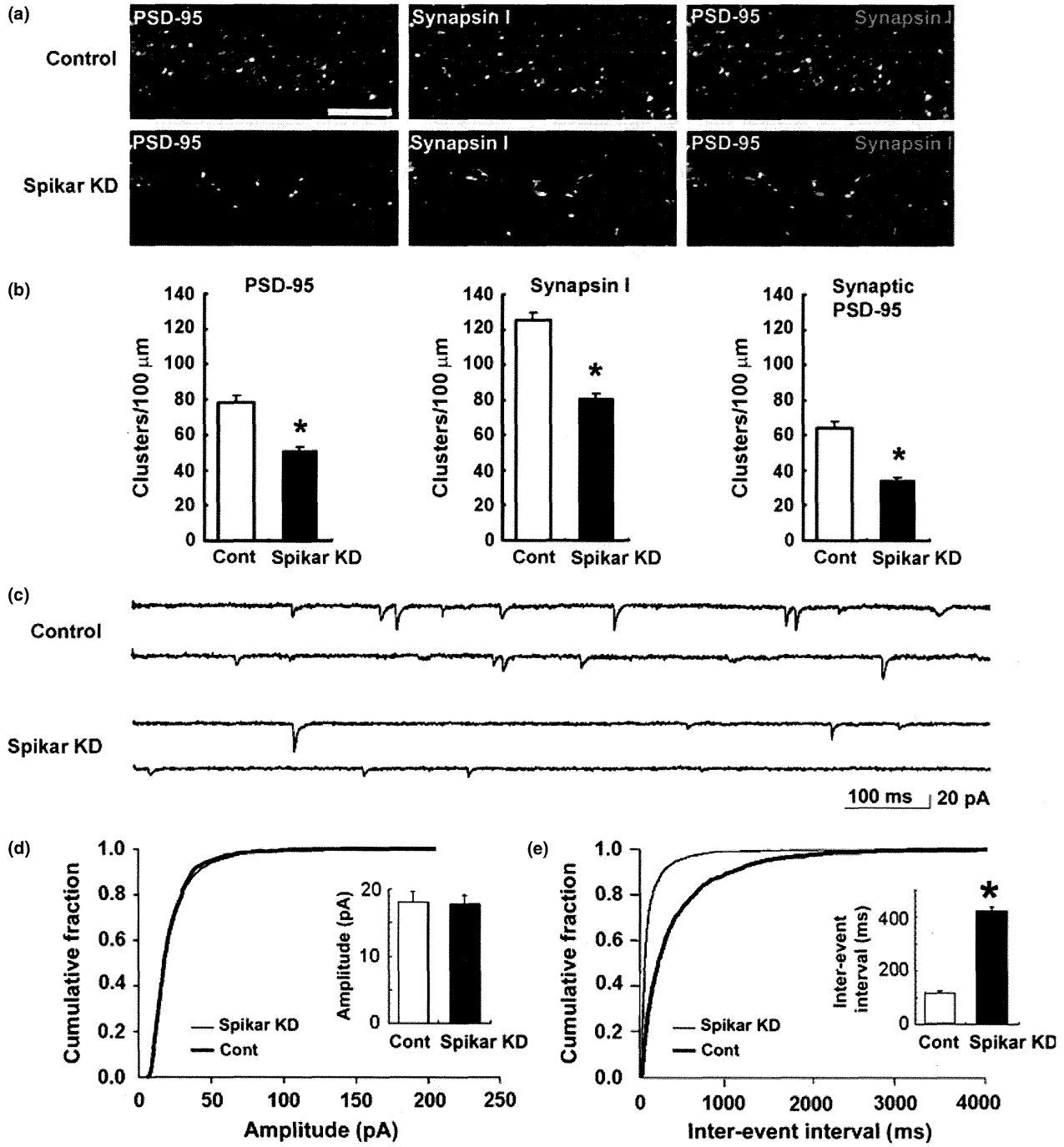

Fig. 4 Knockdown of spikar reduces excitatory synapses. (a) Cultured neurons were transfected with empty vector (cont) or spikar-shRNA-3 at 3 DIV and analyzed at 16 DIV. Spikar-knockdown (KD) neurons were immunolabeled for PSD-95 (green) and Synapsin I (red). Scale bar, 5 μm. (b) Quantification of cluster densities of PSD-95, Synapsin I, and PSD-95/Synapsin I. Data are presented as mean ± SEM (n = 58 and 64 for control and spikar KD, respectively, *p < 0.01, Welch's t-test). Excitatory synapses are defined as synapsin I-positive, PSD-95-positive clusters. (c) Representative recordings of miniature excitatory postsynaptic currents (mEPSCs) from control and spikar-KD neurons. (d, e) Quantification of mEPSC peak amplitudes and mEPSC inter-event intervals from control and spikar-KD neurons. Inset graphs show the mean ± SEM (n = 17 and 16 for control and spikar KD, respectively, *p < 0.01, Welch's t-test).

uted diffusely throughout the dendritic shafts in the drebrin-KD neurons but not in the control neurons (Fig. 6f). To assess the accumulation of spikar in the dendritic spines, the immunofluorescence intensities of myc-spikar were quantified in dendritic spines and shafts, and the ratios of spine to shaft intensities were calculated. The accumulation of myc-

spikar in spines was significantly inhibited by the loss of drebrin (Control spine/shaft intensity, 1.03 ± 0.03; Drebrin KD, 0.61 ± 0.01; $P < 0.01$) and was rescued by co-transfection with an RNAi-resistant drebrin mutant (drebrin^R) (1.86 ± 0.06, $*p < 0.01$ vs. Drebrin KD, Fig. 6g), indicating that the dendritic localization of spikar was dependent on drebrin. However, the C-terminal region of spikar (aa820-1041), which lacks drebrin-binding activity, accumulated in dendritic spines (Figure S9a). Furthermore, the spikar delta-C isoform, which has a drebrin-binding region but lacks the C-terminal region, was not localized in dendritic spines but was solely localized within the nucleus (Figure S9b). Therefore, binding of spikar to drebrin is not always correlated with dendritic spine localization.

Finally, we examined whether spikar affects drebrin localization at dendritic spines (Fig. 6h). In spikar-KD neurons, the percentages of drebrin-positive filopodia and spines in spikar-KD neurons were similar to those in control neurons (Fig. 6i). Furthermore, the drebrin immunofluorescence intensity within drebrin-positive spines was not affected by spikar KD (Fig. 6j). Together, these data indicate that drebrin localization does not depend on spikar, whereas spikar localization does depend on drebrin.

Overexpression of extranuclear spikar facilitates spine formation in a drebrin-dependent manner

To further investigate the function of spikar in the cytoplasm, we performed a spikar gain-of-function experiment by introducing mNLS-spikar into cultured neurons at 8 DIV and measuring the numbers of spines and filopodia at 13 DIV (Fig. 7a). Overexpression of mNLS-spikar significantly increased the densities of both spines and filopodia (Control: 14.9 ± 1.0 spines/100 μm; 33.8 ± 1.5 filopodia/100 μm; mNLS-spikar: 21.9 ± 1.3 spines/100 μm; 46.6 ± 2.0 filopodia/100 μm; $*p < 0.01$, Fig. 7b–d). We then examined whether the spine-formation activity of mNLS-spikar requires the presence of drebrin. We co-transfected mNLS-spikar and drebrin-shRNA into cultured neurons and measured the numbers of spines and filopodia. Drebrin KD (8–13 DIV) abolished the mNLS-spikar-induced increases in spine and filopodia density (Fig. 7b–d). The inhibition of mNLS-spikar function by drebrin KD was

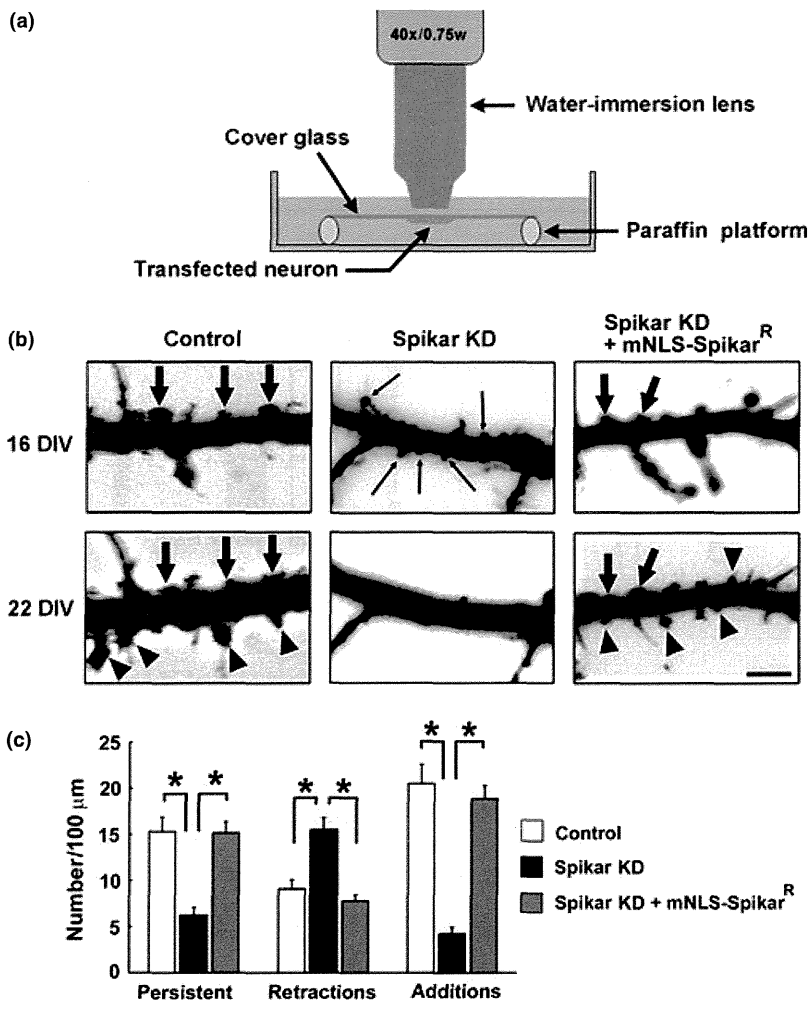

Fig. 5 Live-cell imaging of spikar-knockdown (KD) neurons. (a) Diagram of live-cell imaging method. (b) Cultured neurons were transfected at 8 DIV with empty vector (cont), spikar-shRNA-3, or spikar-shRNA-3+ myc-mutated nuclear localization sequence (mNLS)-spikar^R. Neurons expressing GFP were imaged at 16 and 22 DIV. Arrows indicate spines that were maintained, arrow heads indicate spines that were added, and thin arrows indicate spines that were retracted during the intervening 6-day period. Scale bars, 5 μm. (c) Quantification of the respective fates of spines. Data are presented as mean ± SEM (n = 30, 31, and 47 for control, spikar KD, and spikar KD + myc-mNLS-spikar^R, respectively, $*p < 0.01$, Tukey–Kramer test).

rescued by co-expression of drebrin^R (24.0 ± 1.6 spines/100 μm; 46.4 ± 2.8 filopodia/100 μm; $*p < 0.01$ vs. Drebrin KD + mNLS-spikar). Drebrin KD (8–13 DIV) did not affect the densities of spines and filopodia in the control culture (Fig. 7b–d), although prolonged drebrin-KD (3–16 DIV) decreased the density of spines and filopodia (Control: 45.4 ± 2.1 spines/100 μm; 23.5 ± 1.6 filopodia/100 μm; Drebrin KD: 31.6 ± 2.3 spines/100 μm; 17.7 ± 1.3 filopodia/100 μm; $*p < 0.01$, Figure S10a and b). These data indicate that extranuclear spikar facilitates spine formation, and that this effect requires drebrin.

Discussion

In this study, we identified a novel drebrin-binding protein that we named spikar. Spikar was localized in cell nuclei and acted as a transcriptional co-activator. Intriguingly, in neurons, spikar was localized at dendritic spines in addition to cell nuclei. Using a combination of RNAi knockdown and mNLS-spikar overexpression, we have shown that spikar is involved in the regulation of dendritic spine density.

Role of drebrin in subcellular localization of spikar

Because mNLS-spikar, which can bind to drebrin but lacks a normal NLS, is not localized in the nucleus, drebrin does not seem to be involved in the nuclear localization of spikar. However, drebrin overexpression increases the proportion of cytoplasmic spikar within HEK293 cells, and drebrin KD inhibits the dendritic accumulation of spikar. These data indicate that drebrin is involved in the localization of spikar in dendritic spines. The present study also demonstrates that protein–protein interaction plays a role in the recovery of spikar in the microsomal fraction, which contains drebrin. Moreover, the level of myc-spikar in dendritic spines is correlated with that of drebrin. These data suggest that drebrin anchors spikar in dendritic spines.

Our *in vitro* studies reveal that the N-terminal region of spikar binds to the ADF-H domain of drebrin. Although ADF-superfamily proteins generally bind to actin via the ADF-H domain (Lappalainen *et al.* 1998), drebrin binds to F-actin via the central actin-remodeling region (Hayashi *et al.* 1999; Grintsevich *et al.* 2010). Therefore spikar is not likely to compete with the interaction between drebrin and *F*-actin. We suggest that spikar is included in the drebrin-actin complex in dendritic spines via a direct protein–protein interaction between drebrin and spikar.

However, the delta-C isoform of spikar does not localize to dendritic spines despite the presence of a drebrin-binding domain. In addition, a C-terminal region (amino acids 820–1041) of spikar that does not bind to drebrin accumulates in dendritic spines. These data indicate that drebrin binding is not sufficient for spikar to be localized to dendritic spines, and that besides the direct protein–protein interaction between drebrin and spikar, another mechanism involving the C-terminal region of spikar must also play a role in the accumulation of spikar in dendritic spines.

Extranuclear spikar is involved in dendritic spine formation

The present study indicates that expression of either wild-type spikar or mNLS-spikar can rescue the decreased spine density of spikar-KD neurons. In addition, overexpression of mNLS-spikar increases the spine density of normal cells. Furthermore, our time-lapse imaging data indicate that mNLS-spikar increases the *de novo* formation of spines and decreases the retraction of existing spines in spikar-KD neurons. Because these data indicate that the expression level of extranuclear spikar relates directly to spine density, changes in transcription of other genes, which are likely to be induced by spikar, are not necessary for spine formation. However, we do not deny a possibility of involvement of spikar-mediated transcription in spine formation outright because mNLS-spikar did not rescue the spine density completely. Furthermore, the inhibitory effect of spikar-KD on dendritic branching might affect the formation of spines.

When spine density is decreased by spikar KD, the remaining spines show normal morphologies. In addition, although the frequency of AMPAR-mediated mEPSCs is decreased following spikar KD, the amplitude is not affected. Thus, it is suggested that spikar is involved in the formation

Fig. 6 Drebrin mediates spikar anchoring at dendritic spines. (a) HEK293 cells were transfected with GFP-spikar or GFP-spikar + mDsRED-drebrin. Cytoplasmic GFP-spikar was selectively imaged by subtracting the DAPI signal from GFP images (Subtraction). Scale bar, 50 μm. (b) High magnification image of a co-transfected cell. Scale bar, 20 μm. (c) The ratio of cells possessing cytoplasmic spikar to the total number of transfected cells was significantly increased in the presence of drebrin ($n = 30$ fields, $*p < 0.01$, Mann–Whitney U-test). (d) Cultured neurons were transfected with myc-spikar, and immunostained with myc-spikar (red) and drebrin (green). Scale bars, 30 μm (upper) and 5 μm (lower). (e) Immunofluorescence intensities of myc-spikar and drebrin in spines were significantly correlated ($r = 0.59$, $p < 0.01$). (f) Cultured hippocampal neurons were transfected at 8 DIV with empty vector (cont), or drebrin-shRNA + myc-spikar, or drebrin-shRNA + myc-spikar + HA-drebrin^R. Scale bar, 5 μm. (g) Quantification of the effect of drebrin knockdown (KD) on spine localization of myc-spikar. Data are presented as mean ± SEM ($n > 400$ spines from 30 neurons, $*p < 0.01$, Steel–Dwass test). (h) Cultured neurons were transfected with empty vector (control) or spikar-shRNA-3 (3–16 DIV). Transfected neurons were immunolabeled with antibody for drebrin. Scale bar, 5 μm. (i, j) Quantification of effects of spikar KD on the percentage of drebrin-positive protrusions (i) and the immunofluorescence intensity of drebrin (j). Data are presented as mean ± SEM ($n = 50$ for each group).

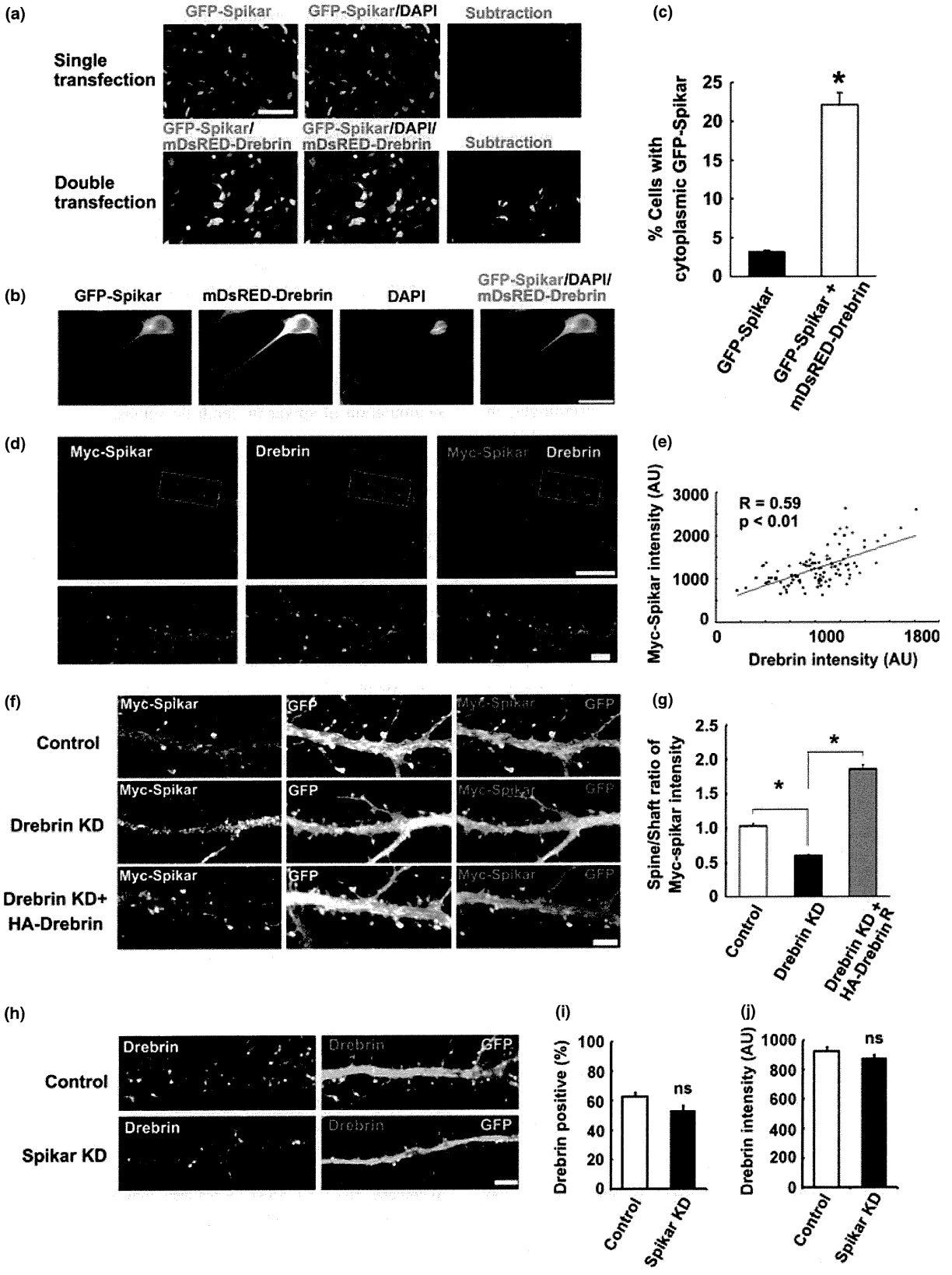
(a)
GFP-Spikar
GFP-Spikar/DAPI
Subtraction
Single transfection
GFP-Spikar/ mDsRED-Drebrin
GFP-Spikar/DAPI/ mDsRED-Drebrin
Subtraction
Double transfection
(b)
GFP-Spikar
mDsRED-Drebrin
DAPI
GFP-Spikar/DAPI/ mDsRED-Drebrin
(c)
% Cells with cytoplasmic GFP-Spikar
25
20
15
10
5
0
*
GFP-Spikar
GFP-Spikar + mDsRED-Drebrin
(d)
Myc-Spikar
Drebrin
Myc-Spikar
Drebrin
(e)
Myc-Spikar intensity (AU)
3000
2000
1000
0
R = 0.59
p < 0.01
0
1000
1800
Drebrin intensity (AU)
(f)
Control
Drebrin KD
Drebrin KD+ HA-Drebrin
Myc-Spikar
GFP
(g)
Spine/Shaft ratio of Myc-spikar intensity
2.5
2.0
1.5
1.0
0.5
0
*
*
Control
Drebrin KD
Drebrin KD+ HA-Drebrin R
(h)
Control
Spikar KD
Drebrin
GFP
(i)
Drebrin positive (%)
100
80
60
40
20
0
ns
Control
Spikar KD
(j)
Drebrin intensity (AU)
1000
800
600
400
200
0
ns
Control
Spikar KD

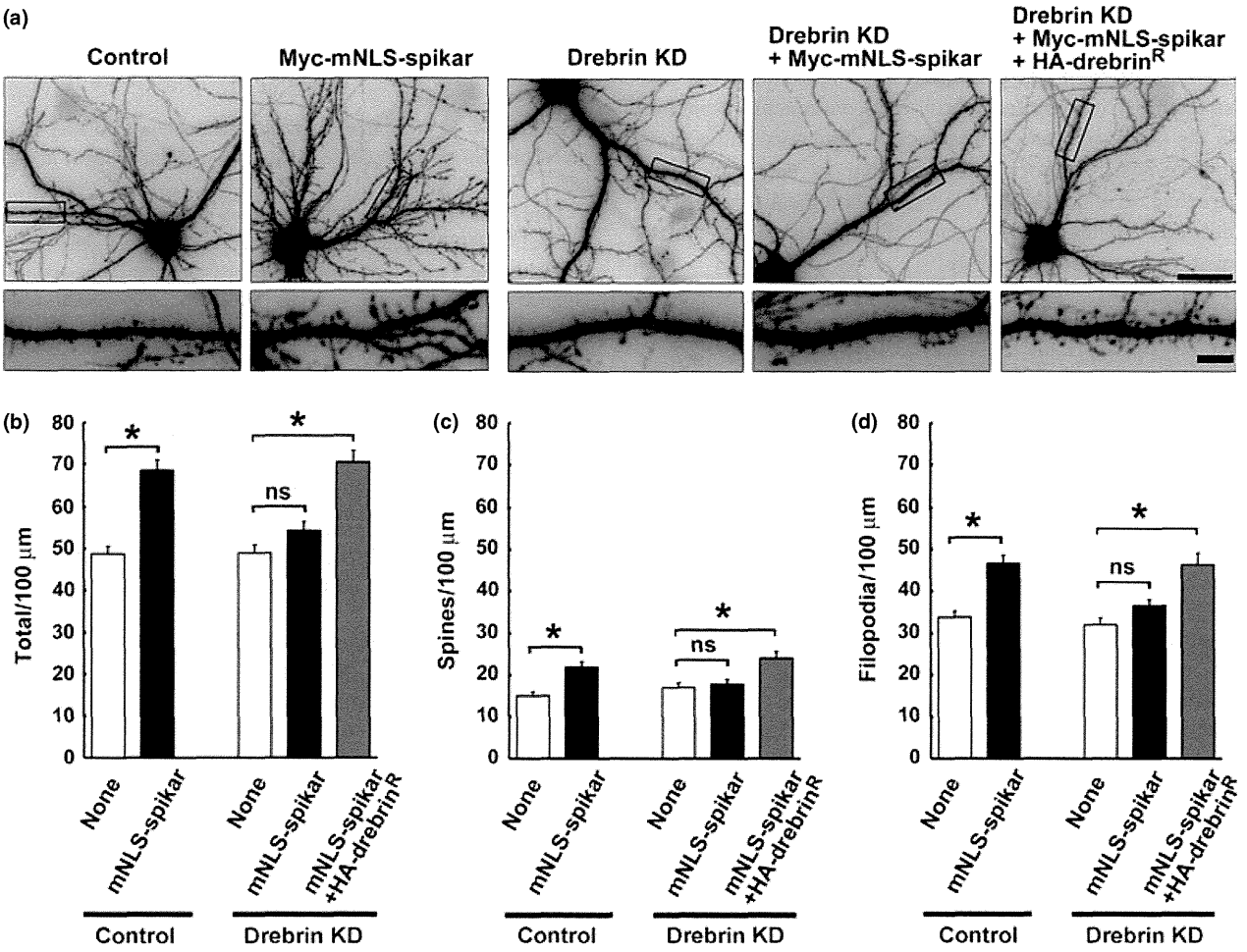

Fig. 7 Effect of extranuclear spikar overexpression is inhibited by drebrin knockdown (KD). (a) Cultured neurons were transfected after 8 DIV with empty vector (control), empty vector + myc-mutated nuclear localization sequence (mNLS)-Spikar, drebrin-shRNA, drebrin-shRNA + myc-mNLS-Spikar, or drebrin-shRNA + myc-mNLS-Spikar + HA-drebrin^R. GFP images were analyzed at 13 DIV. Scale bars, 30 μm (upper); 5 μm (lower). (b–d) Quantification of spine and filopodia density for each experimental condition. Data are presented as mean ± SEM ($n = 55$ for each group, $^*p < 0.01$, Tukey–Kramer test).

and stabilization of dendritic spines, but it is not involved in the function of mature spines.

Role of drebrin–spikar interaction in spine formation

Interestingly, overexpression of mNLS-spikar did not increase spine density in drebrin-KD neurons. This suggests that drebrin-mediated anchoring of spikar through protein-protein interaction at dendritic spines is necessary for increasing spine density. An alternative explanation is that the decrease in spine density caused by drebrin KD counteracts the increase induced by spikar overexpression. We and others have previously shown that drebrin KD inhibits spine formation (Takahashi *et al.* 2006; Biou *et al.* 2008). In fact, we detected a significant decrease in spine density in longer duration (3–16 DIV) drebrin KD. Therefore, spikar might function in a different regulatory pathway from drebrin. However, we did not detect any decrease in spine density in a drebrin-KD experiment of the same duration (8–13 DIV) as the mNLS-spikar overexpression experiment. This result indicates that the likelihood of the latter possibility is low, although it is not known why shorter term drebrin KD (8–13 DIV) did not lead to a decrease in spine density similar to prolonged drebrin KD (3–16 DIV). The reduction of drebrin expression in drebrin KD (8–13 DIV) neurons might be sufficient to block *de novo* spine formation induced by overexpressed mNLS-spikar, but not enough to decrease the spine density compared with the reduction in drebrin KD (3–16 DIV).

While the present study indicates that spikar KD does not affect spine morphology, our previous study demonstrated that drebrin KD does alter spine morphology (Takahashi *et al.* 2006). It has been reported that drebrin accumulates at nascent excitatory postsynaptic sites (Aoki *et al.* 2005) before the accumulation of PSD-95 (Takahashi *et al.* 2003)

and drebrin is suggested to play a pivotal role in forming a unique stable actin structure at postsynaptic sites (Shirao and Gonzalez-Billault 2013). Spikar may be recruited to the actin structure by binding to drebrin, and consequently functions in the spikar-mediated spine density regulatory pathway. In this context, other proteins recruited to the stable actin structure could mediate the morphological changes in dendritic spines, in a manner distinct from the spikar-mediated regulatory pathway.

Several molecules have been reported to be involved in dendritic spine formation and stabilization (McMahon and Diaz 2011). Diacylglycerol kinase (DGK)ζ is a DGK isoform that is enriched at excitatory synapses. DGKζ KD is known to reduce spine stability and density without changing spine morphology (Kim *et al.* 2009). Furthermore, the loss of DGKζ decreases the frequency of mEPSCs without affecting their amplitudes (Kim *et al.* 2009). Because these morphological and electrophysiological phenotypes of DGKζ KD are similar to those of spikar KD, it is suggested that spikar and DGKζ might be involved in a similar pathway regulating dendritic spine formation and stabilization, although an interaction between DGKζ and drebrin has not been reported.

Some cell adhesion molecules are also involved in dendritic spine formation and stabilization. Knockdown of N-cadherin reduces the stability of dendritic spines (Mendez *et al.* 2010), and a dominant-negative disruption of leukocyte common antigen-related (LAR) receptor protein tyrosine phosphatase function increases the retraction of existing spines and decreases *de novo* spine formation (Dunah *et al.* 2005). Although these phenotypes are similar to those of spikar KD, unlike spikar KD, the functional inhibition of N-cadherin or LAR results in formation of smaller dendritic spines. Therefore, spikar is likely to be involved in a different regulatory pathway from N-cadherin or LAR.

Acknowledgments

We thank Dr Ryoki Ishikawa for His6-drebrin. T7 work was supported by Grants-in-Aid for Young Scientists (15700285, 18700306, 21700340) and a Grant-in-Aid for Scientific Research (19200029) from the Japan Society for the Promotion of Science (JSPS). All authors declare that they have no conflict of interest.

Supporting information

Additional supporting information may be found in the online version of this article at the publisher's web-site:

Appendix S1. The expression vectors for TRβ1 and ERα (Takeshita *et al.* 1998), and GR (Iwasaki *et al.* 2001) have been described previously.

Figure S1. (a) The spikar antibody recognized GFP-spikar as a single band at approximately 200 kDa, demonstrating that the spikar antibody specifically recognized spikar protein.

Figure S2. (a) Cultured neurons were transfected with an empty vector (control), luciferase-shRNA, or spikar-shRNA-2 at 3 DIV, and analyzed at 16 DIV.

Figure S3. (a) Higher magnification image of dendritic spines. The neuron is transfected with GFP. Scale bar, 2 μm. (b) Illustration of panel (a).

Figure S4. (a, b) Spikar activated transcription mediated by the glucocorticoid receptor (GR) and estrogen receptor α (ERα) in CV-1 cells.

Figure S5. (e, f) Interaction between drebrin and spikar were assayed by HIS3 induction in the yeast two-hybrid system.

Figure S6. (a, b) Immunofluorescence localization of spikar in cultured GFP-transfected neurons at two developmental stages (7 DIV and 14 DIV).

Figure S7. (a, b) Cultured hippocampal neurons were transfected at 8 DIV with myc-spikar (a) or myc-mNLS-spikar (b), and immunostained with anti-myc antibody at 16 DIV.

Figure S8. Cultured neurons were transfected with an empty vector (cont), spikar-shRNA-3, spikar-shRNA-3 + myc-spikarR, or spikar-shRNA-3 + myc-mNLS-spikarR at 3 DIV and analyzed at 16 DIV.

Figure S9. (a) Cultured neurons were transfected with GFP-spikar (820-1041) at 8 DIV and analyzed at 16 DIV. GFP-spikar (820-1041), which does not bind to drebrin, was localized in dendritic spines. Scale bar, 5 μm.

Figure S10. (a) Cultured neurons were transfected with empty vector (control) or drebrin-shRNA at 3 DIV and analyzed at 16 DIV. Prolonged drebrin KD decreased the density of dendritic spines and filopodia. Scale bars, 30 μm (upper); 5 μm (lower).

References

Aoki C., Sekino Y., Hanamura K., Fujisawa S., Mahadomrongkul V., Ren Y. and Shirao T. (2005) Drebrin A is a postsynaptic protein that localizes in vivo to the submembranous surface of dendritic sites forming excitatory synapses. *J. Comp. Neurol.* **483**, 383–402.

Biou V., Brinkhaus H., Malenka R. C. and Matus A. (2008) Interactions between drebrin and Ras regulate dendritic spine plasticity. *Eur. J. Neurosci.* **27**, 2847–2859.

Dotti C. G., Sullivan C. A. and Banker G. A. (1988) The establishment of polarity by hippocampal neurons in culture. *J. Neurosci.* **8**, 1454–1468.

Dunah A. W., Hueske E., Wyszynski M., Hoogenraad C. C., Jaworski J., Pak D. T., Simonetta A., Liu G. and Sheng M. (2005) LAR receptor protein tyrosine phosphatases in the development and maintenance of excitatory synapses. *Nat. Neurosci.* **8**, 458–467.

Ethell I. M. and Pasquale E. B. (2005) Molecular mechanisms of dendritic spine development and remodeling. *Prog. Neurobiol.* **75**, 161–205.

Fossey S. C., Kuroda S., Price J. A., Pendleton J. K., Freedman B. I. and Bowden D. W. (2000) Identification and characterization of PRKCBP1, a candidate RACK-like protein. *Mamm. Genome* **11**, 919–925.

Gorlich A., Zimmermann A. M., Schober D., Bottcher R. T., Sassoe-Pognetto M., Friauf E., Witke W. and Rust M. B. (2012) Preserved morphology and physiology of excitatory synapses in profilin1-deficient mice. *PLoS ONE* **7**, e30068.

Grintsevich E. E., Galkin V. E., Orlova A., Ytterberg A. J., Mikati M. M., Kudryashov D. S., Loo J. A., Egelman E. H. and Reisler E. (2010) Mapping of drebrin binding site on F-actin. *J. Mol. Biol.* **398**, 542–554.

Hayashi K. and Shirao T. (1999) Change in the shape of dendritic spines caused by overexpression of drebrin in cultured cortical neurons. *J. Neurosci.* **19**, 3918–3925.

Hayashi K., Ishikawa R., Ye L. H., He X. L., Takata K., Kohama K. and Shirao T. (1996) Modulatory role of drebrin on the cytoskeleton within dendritic spines in the rat cerebral cortex. *J. Neurosci.* **16**, 7161–7170.

Hayashi K., Ishikawa R., Kawai-Hirai R., Takagi T., Taketomi A. and Shirao T. (1999) Domain analysis of the actin-binding and actin-remodeling activities of drebrin. *Exp. Cell Res.* **253**, 673–680.

Huttner W. B., Schiebler W., Greengard P. and De Camilli P. (1983) Synapsin I (protein I), a nerve terminal-specific phosphoprotein. III. Its association with synaptic vesicles studied in a highly purified synaptic vesicle preparation. *J. Cell Biol.* **96**, 1374–1388.

Ishikawa R., Hayashi K., Shirao T., Xue Y., Takagi T., Sasaki Y. and Kohama K. (1994) Drebrin, a development-associated brain protein from rat embryo, causes the dissociation of tropomyosin from actin filaments. *J. Biol. Chem.* **269**, 29928–29933.

Ishikawa R., Katoh K., Takahashi A., Xie C., Oseki K., Watanabe M., Igarashi M., Nakamura A. and Kohama K. (2007) Drebrin attenuates the interaction between actin and myosin-V. *Biochem. Biophys. Res. Commun.* **359**, 398–401.

Ivanov A., Esclapez M., Pellegrino C., Shirao T. and Ferhat L. (2009) Drebrin A regulates dendritic spine plasticity and synaptic function in mature cultured hippocampal neurons. *J. Cell Sci.* **122**, 524–534.

Iwasaki T., Chin W. W. and Ko L. (2001) Identification and characterization of RRM-containing coactivator activator (CoAA) as TRBP-interacting protein, and its splice variant as a coactivator modulator (CoAM). *J. Biol. Chem.* **276**, 33375–33383.

Iwasaki T., Miyazaki W., Takeshita A., Kuroda Y. and Koibuchi N. (2002) Polychlorinated biphenyls suppress thyroid hormone-induced transactivation. *Biochem. Biophys. Res. Commun.* **299**, 384–388.

Kato K., Shirao T., Yamazaki H., Imamura K. and Sekino Y. (2012) Regulation of AMPA receptor recruitment by the actin binding protein drebrin in cultured hippocampal neurons. *JNSNE* **1**, 153–160.

Kim K., Yang J., Zhong X. P. *et al.* (2009) Synaptic removal of diacylglycerol by DGKzeta and PSD-95 regulates dendritic spine maintenance. *EMBO J.* **28**, 1170–1179.

Kojima N., Wang J., Mansuy I. M., Grant S. G., Mayford M. and Kandel E. R. (1997) Rescuing impairment of long-term potentiation in fyn-deficient mice by introducing Fyn transgene. *Proc. Natl Acad. Sci. USA* **94**, 4761–4765.

Kwon H. B. and Sabatini B. L. (2011) Glutamate induces de novo growth of functional spines in developing cortex. *Nature* **474**, 100–104.

Lappalainen P., Kessels M. M., Cope M. J. and Drubin D. G. (1998) The ADF homology (ADF-H) domain: a highly exploited actin-binding module. *Mol. Biol. Cell* **9**, 1951–1959.

Mammoto A., Sasaki T., Asakura T., Hotta I., Imamura H., Takahashi K., Matsuura Y., Shirao T. and Takai Y. (1998) Interactions of drebrin and gephyrin with profilin. *Biochem. Biophys. Res. Commun.* **243**, 86–89.

Masselink H. and Bernards R. (2000) The adenovirus E1A binding protein BS69 is a corepressor of transcription through recruitment of N-CoR. *Oncogene* **19**, 1538–1546.

McMahon S. A. and Diaz E. (2011) Mechanisms of excitatory synapse maturation by trans-synaptic organizing complexes. *Curr. Opin. Neurobiol.* **21**, 221–227.

Mendez P., De Roo M., Poglia L., Klauser P. and Muller D. (2010) N-cadherin mediates plasticity-induced long-term spine stabilization. *J. Cell Biol.* **189**, 589–600.

Mizui T., Takahashi H., Sekino Y. and Shirao T. (2005) Overexpression of drebrin A in immature neurons induces the accumulation of F-actin and PSD-95 into dendritic filopodia, and the formation of large abnormal protrusions. *Mol. Cell. Neurosci.* **30**, 630–638.

Rochefort N. L. and Konnerth A. (2012) Dendritic spines: from structure to in vivo function. *EMBO Rep.* **13**, 699–708.

Ryu J., Liu L., Wong T. P., Wu D. C., Burette A., Weinberg R., Wang Y. T. and Sheng M. (2006) A critical role for myosin IIb in dendritic spine morphology and synaptic function. *Neuron* **49**, 175–182.

Sala C., Futai K., Yamamoto K., Worley P. F., Hayashi Y. and Sheng M. (2003) Inhibition of dendritic spine morphogenesis and synaptic transmission by activity-inducible protein Homer1a. *J. Neurosci.* **23**, 6327–6337.

Sala C., Cambianica I. and Rossi F. (2008) Molecular mechanisms of dendritic spine development and maintenance. *Acta. Neurobiol. Exp.* **68**, 289–304.

Sekiguchi T., Hirose E., Nakashima N., Ii M. and Nishimoto T. (2001) Novel G proteins, Rag C and Rag D, interact with GTP-binding proteins, Rag A and Rag B. *J. Biol. Chem.* **276**, 7246–7257.

Sekino Y., Kojima N. and Shirao T. (2007) Role of actin cytoskeleton in dendritic spine morphogenesis. *Neurochem. Int.* **51**, 92–104.

Sharma S., Grintsevich E. E., Phillips M. L., Reisler E. and Gimzewski J. K. (2011) Atomic force microscopy reveals drebrin induced remodeling of f-actin with subnanometer resolution. *Nano Lett.* **11**, 825–827.

Sharma S., Grintsevich E. E., Hsueh C., Reisler E. and Gimzewski J. K. (2012) Molecular cooperativity of drebrin1-300 binding and structural remodeling of F-actin. *Biophys. J .* **103**, 275–283.

Shiraishi Y., Mizutani A., Yuasa S., Mikoshiba K. and Furuichi T. (2004) Differential expression of Homer family proteins in the developing mouse brain. *J. Comp. Neurol.* **473**, 582–599.

Shirao T. and Gonzalez-Billault C. (2013) Actin filaments and microtubules in dendritic spines. *J. Neurochem.* **126**, 155–164.

Shirao T. and Obata K. (1986) Immunochemical homology of 3 developmentally regulated brain proteins and their developmental change in neuronal distribution. *Brain Res.* **394**, 233–244.

Shirao T., Kojima N., Kato Y. and Obata K. (1988) Molecular cloning of a cDNA for the developmentally regulated brain protein, drebrin. *Brain Res.* **464**, 71–74.

Shirao T., Hayashi K., Ishikawa R., Isa K., Asada H., Ikeda K. and Uyemura K. (1994) Formation of thick, curving bundles of actin by drebrin A expressed in fibroblasts. *Exp. Cell Res.* **215**, 145–153.

Sholl D. A. (1953) Dendritic organization in the neurons of the visual and motor cortices of the cat. *J. Anat.* **87**, 387–406.

Takahashi H., Sekino Y., Tanaka S., Mizui T., Kishi S. and Shirao T. (2003) Drebrin-dependent actin clustering in dendritic filopodia governs synaptic targeting of postsynaptic density-95 and dendritic spine morphogenesis. *J. Neurosci.* **23**, 6586–6595.

Takahashi H., Mizui T. and Shirao T. (2006) Down-regulation of drebrin A expression suppresses synaptic targeting of NMDA receptors in developing hippocampal neurones. *J. Neurochem.* **97**(Suppl 1), 110–115.

Takeshita A., Yen P. M., Ikeda M., Cardona G. R., Liu Y., Koibuchi N., Norwitz E. R. and Chin W. W. (1998) Thyroid hormone response elements differentially modulate the interactions of thyroid hormone receptors with two receptor binding domains in the steroid receptor coactivator-1. *J. Biol. Chem.* **273**, 21554–21562.

Tohgi H., Utsugisawa K., Yamagata M. and Yoshimura M. (1995) Effects of age on messenger RNA expression of glucocorticoid, thyroid hormone, androgen, and estrogen receptors in postmortem human hippocampus. *Brain Res.* **700**, 245–253.

第1特集 3

iPS細胞由来マスト細胞を用いた難治性疾患の新規治療薬開発へ向けて

独立行政法人医薬基盤研究所　山口 朋子、川端 健二

Key words　マスト細胞／iPS 細胞／創薬応用／炎症性腸疾患／多発性硬化症

幹細胞と iPS 細胞の違い

幹細胞は、様々な細胞へと分化する能力（多能性）を有しており、適切な条件下で培養することにより、血液細胞、神経細胞、心筋細胞など多種多様な細胞へと分化可能である。したがって、幹細胞は、薬効評価・安全性薬理試験などの創薬スクリーニングや再生医療への応用が期待されている（図1）。

幹細胞のなかでも、とくに人工多能性幹細胞すなわち iPS 細胞は、皮膚などの体細胞に数種の遺伝子を導入することにより樹立されることから、受精卵を用いる ES 細胞（胚性幹細胞）とは異なり、倫理的な問題を回避することができる。また、iPS 細胞は患者自身の細胞から樹立することができるため、移植細胞による拒絶反応の可能性が低いと考えられている。

iPS 細胞の応用においては、神経変性疾患であるパーキンソン病の患者から iPS 細胞を樹立し、目的の細胞に分化させることで、これまで技術的に不可能であっ

Author 著者

山口 朋子（やまぐち ともこ）
独立行政法人
医薬基盤研究所

2010年、大阪大学大学院薬学研究科博士後期課程修了。専門は免疫学。ES/iPS細胞から各種血液・免疫細胞への分化誘導法の確立、マスト細胞の分化・成熟化メカニズムの解明に向けて研究中。日本遺伝子治療学会H23年度アンジェスMG賞。研究室リンク

川端 健二（かわばた けんじ）
独立行政法人医薬基盤研究所
大阪大学大学院薬学研究科

1997年、京都大学大学院薬学研究科博士後期課程薬学専攻修了（薬学博士）。大阪府立母子総合医療センター研究所免疫部門流動研究員、国立医薬品食品衛生研究所遺伝子細胞医薬部研究員などを経て、2005年、独立行政法人医薬基盤研究所　遺伝子導入制御プロジェクト主任研究員に。2010年より独立行政法人医薬基盤研究所幹細胞制御プロジェクトプロジェクトリーダー。専門は血液学。幹細胞の創薬応用を研究中。2012年 第10回産学官連携功労者表彰（厚生労働大臣賞）。研究室リンク

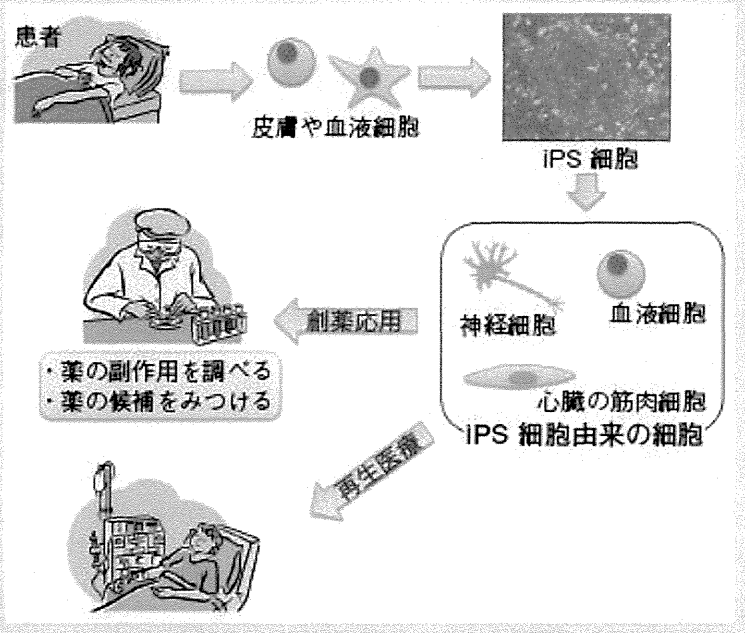

図1　iPS 細胞を用いた臨床応用

た患者の体内組織（パーキンソン病であれば神経細胞）における病態を再現できることが報告されている[1]。

また、アルツハイマー病の患者から樹立したiPS細胞を用いて、青魚に含まれる不飽和脂肪酸の一種がその発症を抑える可能性があることも報告されている[2]。したがって、発症の原因が未だ不明な疾患のメカニズム解明や新規治療薬の開発に、患者由来iPS細胞が有用であることが示されている。他にも、進行性骨化性線維異形成症や原発性免疫不全症候群などの難治性疾患の患者からiPS細胞が樹立され、現在研究が進められている。

難治性疾患とマスト細胞

炎症性腸疾患は、長期にわたり消化管に原因不明の炎症を呈する難治性疾患であり、近年急速に罹患率が増加している。大腸の粘膜にびらんや潰瘍ができる潰瘍性大腸炎や大腸および小腸の粘膜の慢性の炎症、あるいは潰瘍ができるクローン病などは、炎症性腸疾患の代表的な疾患として知られている。

これらの疾患の病因は未だ明らかとなっておらず、現在では遺伝的因子と環境因子が複雑に絡み合っていると考えられている。